

University of Alberta

MODELLING ATMOSPHERE-ICE SHEET FEEDBACKS

by

Michael S. Pritchard



A thesis submitted to the Faculty of Graduate Studies and Research in partial fulfillment of the requirements for the degree of **Master of Science**.

Department of Earth and Atmospheric Sciences

Edmonton, Alberta  
Fall 2006



Library and  
Archives Canada

Bibliothèque et  
Archives Canada

Published Heritage  
Branch

Direction du  
Patrimoine de l'édition

395 Wellington Street  
Ottawa ON K1A 0N4  
Canada

395, rue Wellington  
Ottawa ON K1A 0N4  
Canada

*Your file* *Votre référence*  
*ISBN: 978-0-494-22348-2*  
*Our file* *Notre référence*  
*ISBN: 978-0-494-22348-2*

#### NOTICE:

The author has granted a non-exclusive license allowing Library and Archives Canada to reproduce, publish, archive, preserve, conserve, communicate to the public by telecommunication or on the Internet, loan, distribute and sell theses worldwide, for commercial or non-commercial purposes, in microform, paper, electronic and/or any other formats.

The author retains copyright ownership and moral rights in this thesis. Neither the thesis nor substantial extracts from it may be printed or otherwise reproduced without the author's permission.

#### AVIS:

L'auteur a accordé une licence non exclusive permettant à la Bibliothèque et Archives Canada de reproduire, publier, archiver, sauvegarder, conserver, transmettre au public par télécommunication ou par l'Internet, prêter, distribuer et vendre des thèses partout dans le monde, à des fins commerciales ou autres, sur support microforme, papier, électronique et/ou autres formats.

L'auteur conserve la propriété du droit d'auteur et des droits moraux qui protègent cette thèse. Ni la thèse ni des extraits substantiels de celle-ci ne doivent être imprimés ou autrement reproduits sans son autorisation.

---

In compliance with the Canadian Privacy Act some supporting forms may have been removed from this thesis.

Conformément à la loi canadienne sur la protection de la vie privée, quelques formulaires secondaires ont été enlevés de cette thèse.

While these forms may be included in the document page count, their removal does not represent any loss of content from the thesis.

Bien que ces formulaires aient inclus dans la pagination, il n'y aura aucun contenu manquant.

  
**Canada**

# Abstract

Interactions between the atmosphere and continental ice sheets are explored in the context of several coupled and uncoupled numerical experiments with a thermo-mechanic ice sheet model (ISM) and an atmospheric general circulation model (AGCM). Based on an evaluation of the ISM response to idealized forcing by interannual atmospheric variability at the Last Glacial Maximum (LGM) and millennial scale variability thereafter, we motivate a need for interactive coupling between these two climate components. A novel, fully interactive asynchronous AGCM-ISM coupling scheme is therefore developed and applied to ice sheet deglaciation simulations. We find that this interactive AGCM coupling scheme can lead to dramatically enhanced ISM performance, provided the radiative feedbacks permitted by the coupling infrastructure include a representation of seasonal ice albedo changes.

# Contents

<b>1</b>	<b>Introduction</b>	<b>1</b>
	Bibliography . . . . .	4
<b>2</b>	<b>Estimating the influence of interannual atmospheric variability on the maintenance of continental ice sheets</b>	<b>6</b>
2.1	Introduction . . . . .	6
2.2	Model Description . . . . .	8
2.2.1	Ice Sheet Model . . . . .	8
2.2.2	Atmosphere-Ocean GCM . . . . .	9
2.3	Ice Sheet Simulations . . . . .	12
2.4	Results . . . . .	13
2.4.1	ENSO at the LGM . . . . .	13
2.4.2	Effects of ENSO on the Laurentide Ice Sheet at the LGM	15
2.5	Conclusions . . . . .	17
	Bibliography . . . . .	29

<b>3 Interactive atmosphere-ice coupling</b>	<b>32</b>
3.1 Introduction . . . . .	32
3.2 Model Description . . . . .	34
3.2.1 Atmospheric Model . . . . .	34
3.2.2 Ice Sheet Model . . . . .	35
3.2.3 AGCM-ISM coupling scheme . . . . .	37
3.2.4 A seasonal ice albedo parameterization . . . . .	38
3.3 Description of simulations . . . . .	39
3.4 Results . . . . .	41
3.5 Conclusions . . . . .	42
Bibliography . . . . .	52
<b>4 General Discussion and Conclusions</b>	<b>55</b>
<b>Bibliography</b>	<b>57</b>

# List of Figures

2.1	Global DJF El Niño anomalies as simulated by the GFDL AO-GCM for present-day conditions. El Niño climate perturbations are shown for a) the 30-m air temperature, b) precipitation and c) the 200 hPa stream function. . . . .	19
2.2	Climatological 30-m winds over in the vicinity of the Laurentide ice sheet. The contours show Laurentide ice sheet topography.	20
2.3	Annually averaged El Niño anomalies from the AO-GCM LGM climatology, shown over the Laurentide ice sheet for a) the 30-m air temperature and b) precipitation. The color scales shown only represent the range of variability over the ice sheet. These temperature and precipitation anomalies were used to drive the EN ice sheet simulation. . . . .	21
2.4	As in Figure 2.3, but for LGM La Niña conditions. These temperature and precipitation anomalies were used to drive the LN ice sheet simulation. . . . .	22
2.5	Temperature and thickness time series showing the equilibration of the Laurentide ice sheet to LGM climate simulated by an AO-GCM over a period of 57 kyr. . . . .	23
2.6	As in Figure 2.1, but for LGM El Niño conditions. . . . .	24
2.7	DJF El Niño anomalies of a) sea surface temperature and b) sea ice thickness for the AO-GCM LGM simulation. Sea ice margins for El Niño conditions are represented by the solid red contour, whilst the dashed contour depicts the climatological DJF sea ice margin. . . . .	25

2.8	Laurentide ice sheet anomalies showing changes in a) final ice thickness, b) average ice accumulation and c) average ice ablation over the model domain for a 5 kyr simulation (EN) forced by El Niño-perturbed LGM climatology. . . . .	26
2.9	As in Figure 2.8, but for a 5 kyr simulation (LN) forced by La Niña-perturbed LGM climatology. . . . .	27
2.10	Laurentide ice sheet thickness anomalies showing changes in the final state due to combined El Niño and La Niña LGM climatological forcing for two 5 kyr ice sheet simulations. Figure 2.10a shows results from the ENLN simulation (in which ENSO seasonal variability was neglected), whereas Figure 2.10b is from the ENLN-S simulation, and retains monthly variability in the LGM ENSO signal. . . . .	28
3.1	Schematic of the asynchronous ISM-AGCM coupling scheme. Atmospheric dynamics are equilibrated to a given ice sheet topography on a timescale of 20 years. The resultant climatological annual cycle of surface air temperature and precipitation are sent back to the ISM to drive the following 1000 years of ice evolution, and the process repeated. . . . .	44
3.2	Time series of the monthly global-average eddy kinetic energy from a representative equilibration simulation of the Community Atmosphere Model v3.0 in response to an imposed Laurentide ice sheet topographic state. The choice of a 20 year atmospheric equilibration timescale is justified by the lack of an overall trend in this plot, and the demonstrated sampling of atmospheric interannual variability. . . . .	45
3.3	Ice albedo parameterization as a function of cumulative annual snowmelt. Regions of high snowpack melt (e.g. the summertime ablation zone) darken to a threshold of 0.4, whereas low melt regions (e.g. the ice sheet interior) remain snow-covered and reflective. A uniform ice albedo of 0.5 is imposed upon complete removal of the snowpack (S=0). This scheme was incorporated into the 2WAY-GHG+ALB coupled simulation. . . . .	46

3.4	Monthly ice albedo maps computed during a representative ISM simulation of the Laurentide ice sheet that incorporates the new melt-based ice albedo parameterization depicted in Figure 3.3. The darkening of ice in the marginal ablation zone is clearly evident as the snowpack melts in this region during the transition to summer. . . . .	47
3.5	Initial ice thickness state of the Laurentide ice sheet, used to initialize the Marshall and Clarke ISM for all ice sheet simulations in the present study. . . . .	48
3.6	As in Figure 3.5, but for the initial ice flow state. . . . .	47
3.7	Volume (black lines; $10^6$ km <sup>3</sup> ) and area (blue lines; $10^6$ km <sup>2</sup> ) time series comparing the 1WAY-GHG (solid lines; high greenhouse gas, modern orbital parameters) and 1WAY-INS (dashed lines; low greenhouse gases, 10kyr BP maximum summer insolation) ice sheet simulations. Neither of the idealized warm atmosphere configurations produced appreciable melting under one-way climate forcing. . . . .	49
3.8	Volume (black lines; $10^6$ km <sup>3</sup> ) and area (blue lines; $10^6$ km <sup>2</sup> ) time series comparing the 1WAY-GHG (solid lines; high greenhouse gas, modern orbital parameters) and 2WAY-GHG (dashed lines; same configuration as 1WAY-GHG but with interactive ice-atmosphere coupling enabled) ice sheet simulations. Asynchronous ice-atmosphere coupling points in the 2WAY-GHG experiment are denoted by triangles. Inclusion of two-way ice-atmosphere coupling did not result in an increased melt response to the idealized high greenhouse gas warm atmospheric state. . . . .	50

3.9 Volume (black lines;  $10^6 \text{ km}^3$ ) and area (blue lines;  $10^6 \text{ km}^2$ ) time series comparing the 2WAY-GHG (solid lines; uses an AGCM-ISM coupling scheme with constant ice albedos) to the 2WAY-GHG+ALB (dashed lines; uses an AGCM-ISM coupling scheme that incorporates a seasonal ice albedo parameterization). Asynchronous ice-atmosphere coupling points are denoted by triangles. The inclusion of a seasonal ice albedo parameterization in the coupling scheme results in the expected large ISM melt response to this idealistically warm atmospheric state. Due to computational and time constraints, the 2WAY-GHG+ALB run was executed for a significantly shorter time period than the 2WAY-GHG simulation. . . . . 51

# Chapter 1

## Introduction

Dynamic and thermodynamic interactions between continental ice sheets and the atmosphere have the capacity to generate climate variability on centennial to millennial timescales (Crowley and North, 1990; Crowley, 1984). For instance, ice sheet topography can pose a significant obstacle to atmospheric flow such that large scale ice sheet deformation induces changes in the overlying atmospheric transport of heat and precipitation (Manabe and Broccoli, 1985; Roe and Lindzen, 2001; Bromwich *et al.*, 2004), which in turn affects the ice sheet shape by altering the regional mass balance. Understanding these sorts of feedbacks and the processes that control them is an important question for the climatological community, both in regards to the evolution of ice sheets in the Earth's past and the future evolution of the Greenland and Antarctic ice sheets.

Although much progress has been made in recent years towards the reconstruction from proxy data of climatic conditions since the Last Glacial Maximum (LGM), the lack of detailed millennial timescale records precludes any inferences from being made about ice-atmosphere feedbacks during a glacial cycle. Numerical ice sheet models (ISMs) and climatic general circulation models (GCMs) are thus the only tools available for studying the interactions of these two important components of the climate system. Unfortunately, the substantial discrepancy in timescales of ice versus air flow has long hindered the coupling of traditional cryospheric and atmospheric numerical models. Instead, ice sheet models have to date been predominantly driven by non-interactive seasonally varying climate fields (e.g. Bromwich *et al.*, 2004; Lunt

*et al.*, 2004; Kim, 2004; Shinn and Barron, 1989; Huybrechts *et al.*, 2002, 2004). Models of the atmospheric circulation likewise contain static ice sheet boundary conditions (e.g. Parizek and Alley, 2004; Forsstrom *et al.*, 2003; Forsstrom and Greve, 2004; Huybrechts *et al.*, 2004; Ridley *et al.*, 2005). Accordingly, many plausible radiative and dynamic ice-atmosphere feedback processes are not incorporated into numerical modeling studies of ice sheet and atmospheric evolution.

The research presented here addresses this inadequacy on two fronts. First, in Chapter 2, we demonstrate that it is possible for modes of interannual atmospheric variability to drive lower frequency (millennial scale) ice sheet deformation. This is achieved through a series of ice sheet simulations forced by ENSO climate anomalies from an offline simulation of the LGM. This analysis of the influence of non-seasonal atmospheric variability on millennial scale ice sheet evolution is unexplored territory; we conclude from our modeling study that such variability may have had a significant effect on ice sheet evolution in the Earth's past.

Second, in Chapter 3, we highlight a potential pitfall of the conventional "one-way" climate forcing paradigm that is commonly employed in the ice sheet modeling community through the presentation of an unrealistically insensitive ISM melt response to idealized warm atmospheric conditions. In this thesis, we improve the fidelity of the ice sheet model response to atmospheric conditions through the development of a novel asynchronous interactive atmospheric coupling scheme that is integrable on millennial timescales. This approach to coupled atmosphere-ice sheet modeling is to our knowledge the first of its kind. Crucial to its success is the incorporation into the two-way coupling infrastructure of a new seasonal ice albedo parameterization that improves upon the standard radiative treatment for ice-covered land surfaces in atmospheric GCMs. Without the introduction of this interactive albedo parameterization, two-way coupling offers little advantage to the conventional approach. With it, however, the ISM melt response to idealized warm atmospheric conditions is vastly improved.

Both of the papers presented in this thesis constitute an important step

forward in the emerging field of coupled ice sheet-atmospheric numerical modeling.

# Bibliography

- Bromwich, David H., Toracinta, E. Richard, Wei, H., Oglesby, Robert J., Fastook, James L., Hughes, Terence J., 2004, "Polar MM5 simulation of the winter climate of the Laurentide ice sheet at the LGM", *Journal of Climate*, **17**, 3415–3433
- Crowley, T. J., 1984, "Atmospheric circulation patterns during glacial inception - a possible candidate", *Quaternary Research*, **21**, 105–110
- Crowley, Thomas J., North, Gerald R., 1990, *Paleoclimatology*, Oxford University Press, Inc., New York
- Forsstrom, P. L., Sallasmaa, O., Greve, R., Zwinger, T., 2003, "Simulation of fast-flow features of the Fennoscandian ice sheet during the Last Glacial Maximum", *Annals of Glaciology*, **37**, 383–389
- Forsstrom, Pirjo-Leena, Greve, Ralf, 2004, "Simulation of the Eurasian ice sheet dynamics during the last glaciation", *Global and Planetary Change*, **42**, 59–81
- Huybrechts, P., Janssens, I., Pocin, C., Fichet, T., 2002, "The response of the Greenland ice sheet to climate changes in the 21st century by interactive coupling of an AOGCM with a thermomechanical ice-sheet model", *Annals of Glaciology*, **35**, 409–415
- Huybrechts, P., Gregory, J., Janssens, I., Wild, M., 2004, "Modelling Antarctic and Greenland volume changes during the 20th and 21st centuries forced by GCM time slice integrations", *Global and Planetary Change*, **42**, 83–105
- Kim, S. J., 2004, "The effect of atmospheric CO<sub>2</sub> and ice sheet topography on LGM climate", *Climate Dynamics*, **22**, 639–651
- Lunt, Daniel J., de Noblet-Ducoudr, Nathalie, Charbit, Sylvie, 2004, "Effects of a melted Greenland ice sheet on climate, vegetation, and the cryosphere", *Climate Dynamics*, **23**, 679–694
- Manabe, S., Broccoli, A. J., 1985, "The influence of continental ice sheets on the climate of an ice-age", *Journal of Geophysical Research - Atmospheres*, **90**, 2167–2190
- Parizek, Byron R., Alley, Richard B., 2004, "Implications of increased Greenland surface melt under global-warming scenarios: ice-sheet simulations", *Quaternary Science Reviews*, **23**, 1013–1027
- Ridley, J. K., Huybrechts, P., Gregory, J. M., Lowe, J. A., 2005, "Elimination of the Greenland ice sheet in a high CO<sub>2</sub> climate", *Journal of Climate*, **18**, 3409–3427

Roe, G. H., Lindzen, R. S., 2001, "The mutual interaction between continental-scale ice sheets and atmospheric stationary waves", *Journal of Climate*, **14**, 1450–1465

Shinn, Richard A., Barron, Eric J., 1989, "Climate sensitivity to continental ice sheet size and configuration", *Journal of Climate*, **2**, 1517–1537

## Chapter 2

# Estimating the influence of interannual atmospheric variability on the maintenance of continental ice sheets

### 2.1 Introduction

Although high frequency climate variability on the annual to subannual scale is reasonably well understood, there is an ongoing effort in the community to account for observed low frequency climate variability on the interdecadal to millennial scales. A recent approach that has helped to address this problem is the incorporation of higher-frequency external forcing mechanisms into models of lower frequency processes. Several such studies have provided useful insight into the evolution of slow modes in the ocean (e.g. Goosse and Renssen, 2004), in the coupled atmosphere-ocean system (e.g. An and Wang, 2005; van der Avoird *et al.*, 2002; Schneider and Comuelle, 2005; Newman *et al.*, 2003) and in solid earth systems (e.g. Berger and von Rad, 2005). It has become apparent from such studies that the influence of higher frequency processes on low frequency climate variability is not well represented stochastically. Rather, the well-defined spatial and temporal patterns of higher frequency phenomena such as baroclinic eddies result in coherent forcing of low frequency climate variability that is fundamentally non-random.

In contrast, there is a relative absence of high-to-low frequency coupled studies that deal with cryospheric processes even though this technique has

considerable potential for untangling the dynamic history of massive continental ice sheets in the Earth's past. Initial progress has been made by forcing thermo-mechanic ice sheet models (ISMs) with seasonally varying GCM-derived climatological fields, a technique that has proven to be instrumental in producing reconstructions of the Laurentide Ice Sheet at the Last Glacial Maximum (LGM) (e.g. Marshall *et al.*, 2002; Huybrechts *et al.*, 2004) and the possible fate of the Greenland ice sheet (Otto-Bliesner *et al.*, 2006). However, this approach is limited by the fact that it only takes into account a single frequency of external atmospheric forcing: the annual cycle.

However, as is the case in modern climate, interannual frequencies are likely to have played an important role in glacial climates. Of particular note, the El Niño / Southern Oscillation (ENSO) appears to have been present in the LGM climate (Tudhope *et al.*, 2001) and since in contemporary climate it has a detectable impact on Arctic cryospheric processes (Slonosky *et al.*, 1997) it is likely to have affected glaciated regions. ENSO signatures have been observed in tropical SST proxies (Tudhope *et al.*, 2001; Stott *et al.*, 2002; Koutavas *et al.*, 2002) as well as in paleoclimate AOGCM simulations (Rosenthal and Broccoli, 2004; Bush, 2006). Furthermore, tropical SST anomalies at the LGM triggered atmospheric teleconnection patterns over North America with mass balance implications as high as 1 m/yr for the Laurentide ice sheet (Yin and Battisti, 2001).

Since the net sum of El Niño and La Niña teleconnection anomalies over North America is non-zero, it is highly plausible that interannual variations associated with ENSO may have had a significant influence on the millennial-scale dynamic evolution of ice sheets at the LGM. This possibility is addressed in the present study through a series of simulations of the Laurentide ice sheet forced by simulated atmospheric ENSO teleconnection patterns over North America. Due to computational constraints, a 5000 year interannually-varying record of AO-GCM temperature and precipitation maps is not realizable as an ice sheet forcing. As a first-order attempt to investigate the potential importance of interannual ENSO variability on Laurentide ice sheet dynamics, we therefore investigate the effect of forcing an ice sheet model (ISM) with an-

nual cycle AO-GCM LGM climatology perturbed by persistent regional ENSO climate anomalies.

Section 2.2 provides an overview of the thermo-mechanic ISM and AO-GCM employed in the study, followed by a description of the various ice sheet simulations in Section 2.3. In Section 2.4.1, the global ENSO signature simulated by the AOGCM at the LGM is compared to a present-day control simulation, and characteristic anomaly patterns over North America are discussed. The effects of these teleconnections on the simulated Laurentide ice sheet dynamics are presented and discussed in Section 2.4.2, and several conclusions are summarized in Section 2.5.

## 2.2 Model Description

### 2.2.1 Ice Sheet Model

The numerical ISM used in this study is a three dimensional thermo-mechanic formulation similar to that developed by Huybrechts (1990). Detailed discussions of the model equations and parameterizations are presented in Marshall and Clarke (1997) and Marshall *et al.* (2002). The model employs a set of rheologically constrained conservation equations for energy, mass and momentum in order to simulate the large-scale diffusion of heat (after Mahaffy, 1976) and mass (based on Janssen, 1977) within the ice sheet. Evolving ice loads are interactively coupled to an isostatic mantle-lithosphere model based on Wu and Peltier (1982) and Peltier (1985). Ice sheet mass balance is calculated using the monthly positive degree-day parameterization of Braithwaite (1984). Several parameterizations are employed to represent various uncertain processes in ice sheet modeling including basal sliding and marine iceberg calving (Marshall *et al.*, 2000). Although these parameterizations necessarily have an effect on ice movement, as illustrated in the detailed parameter sensitivity study of Marshall *et al.* (2002), the large-scale dynamics are primarily controlled by climatological boundary conditions imposed at the ice sheet surface. Due to the seasonality of ablation and accumulation, this forcing is imposed through a set of monthly mean temperature and precipitation fields representing the

climatological annual cycle. The temperature field is specified for a given pressure level in the atmosphere and linearly interpolated to the ice surface assuming a constant atmospheric lapse rate of 6 °C/km based on the findings of several previous degree-day glaciological modeling studies (Bran and Hock, 2004; Jóhannesson *et al.*, 1995; Trombotto *et al.*, 1997).

### 2.2.2 Atmosphere-Ocean GCM

The atmosphere-ocean model used to force the three dimensional ISM in this study is a combination of the hybrid spectral atmospheric GCM of Gordon and Stern (1982) and a three-dimensional finite difference primitive equation ocean GCM (Bryan, 1969; Pacanowski *et al.*, 1991), both of which were developed at the Geophysical Fluid Dynamics Laboratory (GFDL) in Princeton. The atmospheric model has 14 vertical levels using the terrain-following  $\sigma$ -coordinate system with horizontal resolution limited by rhomboidal truncation at zonal wavenumber 30 whereas the oceanic component has 15 variably spaced vertical levels with a horizontal resolution of 2 °C in latitude and 3.62 °C in longitude. Oceanic vertical mixing is parameterized globally using the Richardson number scheme of Pacanowski and Philander (1981) and sea ice is modeled after Fanning and Weaver (1996).

The GFDL AO-GCM produces realistic ENSO variability in response to present-day climatological forcing (Bush, 2006). Figure 2.1 shows DJF El Niño anomalies of surface air temperature (TAS), precipitation (PR) and the 200 hPa stream function (STR) extracted from a 70 year simulation of modern climate. The regional distribution of El Niño temperature and precipitation anomalies in the AO-GCM is largely in agreement with modern reconstructions based on observations (AchutaRao and Sperber, 2002) although the magnitude of the thermal response is underestimated most likely because of the relatively coarse model resolution. In addition to the classic eastward motion of the tropical Pacific warm pool, areas observed to experience drought during El Niño such as South Africa, Australia, Indonesia and the Amazon Basin are congruous with warm and dry El Niño anomalies in the AO-GCM simulation. In comparison to previous simulations, the Richardson number vertical mixing

scheme in the ocean GCM has greatly improved the GFDL coupled model's ability to simulate realistic modern ENSO variability (Pacanowski and Philander, 1981). Although some underestimation of regional warming occurs over the eastern tropical Pacific and western Canada/Alaska, the overall quality of the simulated present-day ENSO teleconnection patterns is quite good compared to other coupled AO-GCMs (AchutaRao and Sperber, 2002).

The dynamic origins of atmospheric teleconnections over North America associated with ENSO are of particular importance to the present study. A variety of modern observations indicate that during boreal wintertime El Niño, Alaska and western Canada experience warmer weather while cooler, wetter conditions prevail over the eastern seaboard (Rasmusson and Carpenter, 1982). These changes are accompanied by large-scale spatial anomalies in the mid-tropospheric geopotential height field that appear to be associated with preferred modes of atmospheric planetary wave activity excited during El Niño, such as the Pacific North American (PNA) pattern (Straus and Shukla, 2002). Early results from linear theory proposed that PNA-like variability could be caused by a stationary Rossby "wave train" excited in the subtropical mid-troposphere during El Niño by an increase in divergent outflow over the shifted tropical Pacific warm pool (Sardeshmukh and Hoskins, 1988). This notion is supported by the observation of a strong Rossby wave response during El Niño in the real atmosphere (Philander, 1990, p. 32). Figure 2.1c demonstrates an analogous dynamical response during El Niño in the GFDL AO-GCM; a pair of anomalous anticyclonic flow patterns is evident in the 200 hPa stream function, straddling the equator over the Pacific warm pool. The northernmost portion of this anomaly reinforces the subtropical jet during El Niño in the AO-GCM, influencing the advection of low latitude air over western North America. Also evident is an equatorially trapped Kelvin wave response, evident in the 200 hPa stream function as symmetric westerly flow along the equator. Convergence of the Rossby wave and Kelvin wave responses leads to upper level convergence, subsidence, and drying of Indonesia and Australia. More recent studies on the dynamics of ENSO teleconnections have investigated the effects of transient eddies, diabatic cooling processes (DeWeaver and

Nigam, 2004; Trenberth *et al.*, 2002) and sources of nonlinear ENSO variability (e.g. Hannachi, 2001; Wu and Hsieh, 2004), all of which likely contribute to the development of preferred modes of atmospheric variability over North America. Although a review of this evolving branch of atmospheric research is beyond the scope of this study, it is important to note that atmospheric teleconnections over North America associated with ENSO arise from a number of complicated dynamic processes.

The climate of the Last Glacial Maximum has been studied extensively using the GFDL AO-GCM for 15-year and 70-year simulations (Bush and Philander, 1999; Bush, 2006). These studies document a global average cooling signal of 4.3 °C compared to present-day conditions, due primarily to cooling over the North American and Eurasian ice sheets. Changes in climatological winds simulated at the LGM include a strengthening of the tropical Pacific easterlies, increased cyclonic activity over the northwest Atlantic and a weakening of the south Asian summer monsoon. Of particular note, the Laurentide ice sheet has a significant effect on the low-level circulation over North America (Figure 2.2). The massive topography of the Laurentide ice sheet acts as an obstacle to low-level atmospheric flow, effectively splitting the surface signature of the westerly mid-latitude jetstream into a dual-branch structure that circumnavigates the ice sheet perimeter. The fast-flowing northern and southern branches of this midlatitude “split jetstream” recombine downstream of the ice sheet into a single broad band of intense westerly wind over the North Atlantic. A strong anticyclonic signature is superimposed over the cool ice sheet interior on this branched surface wind environment, as is observed over the Greenland and Antarctic ice sheets today.

In order to investigate the effects of ENSO on Laurentide ice sheet dynamics at the LGM, temperature and precipitation data subsets were isolated for those months matching the El Niño / La Niña tropical sea surface temperature (SST) criteria of the NINO-3.4 region (Trenberth, 1997). Composite anomaly maps were then formed by averaging over these months (see Figures 2.3 and 2.4). It is prudent to note that the definition of El Niño and La Niña months in the tropical Pacific (i.e. SST anomalies must exceed 0.4 °C for 6 months) gives rise

to a nonlinear relationship between associated El Niño and La Niña anomalies in the extratropics.

### 2.3 Ice Sheet Simulations

In order to investigate the effects of ENSO on ice sheet dynamics, five 5-kyr ice sheet simulations were carried out using different climatological temperature and precipitation forcing maps derived from the AO-GCM LGM simulation. The ice sheet model was initialized with a linear vertical temperature profile and an LGM Laurentide ice sheet thickness distribution obtained from the ISM simulation of Marshall and Clark (2002). Internal temperatures were subsequently equilibrated to LGM conditions over the course of a 57 kyr spin-up simulation forced by seasonal temperature and precipitation climatology from the AO-GCM. Figure 2.5 shows time series of domain-averaged ice thickness and temperature fields during this equilibration process. The relatively rapid equilibration of the ice sheet to LGM climatological forcing indicates that the initial bulk ice sheet topography was consistent with the simulated AO-GCM climate, despite some small regional mass balance adjustments.

The first simulation was a control run in which the Laurentide ice sheet dynamics were forced by the LGM annual cycle climatology alone. In the next two ice sheet simulations (EN/LN) the annual cycle climate forcing was perturbed by composite maps of precipitation and temperature anomalies associated with both the El Niño and La Niña climate states extracted from the LGM simulation (Figure 2.3). Although the El Niño and La Niña composite anomalies are somewhat antisymmetric over the Laurentide ice sheet, they are not exact opposites and therefore their combined effect is nonzero. Accordingly, the net effect of high frequency, interannually varying ENSO teleconnections over North America at the LGM is a climate forcing with a well defined spatial structure. A fourth run dubbed ENLN was therefore conducted which investigated the ice sheet's dynamic response to the averaged El Niño / La Niña climatic perturbation. In this case, the imposed LGM annual cycle climatology was perturbed by an average of the EN and LN annual cli-

mate anomalies. This experiment was then repeated using seasonally varying ENSO teleconnection patterns in a fifth and final run named ENLN-S in order to determine the sensitivity of the ice sheet response to ENSO seasonality.

## 2.4 Results

### 2.4.1 ENSO at the LGM

Figure 2.6 shows the simulated LGM DJF El Niño anomalies of near surface air temperature, precipitation and 200 hPa streamfunction. The extratropical thermal response to winter El Niño conditions at the LGM is much more pronounced at high latitudes than it is today (cf. Figure 2.1a), increasing in amplitude by a factor of 3 over the Antarctic and Arctic regions with a mean peak warming of 3 °C over the Laptev and East Siberian seas. Warming in the central tropical Pacific at the LGM is less than for modern El Niño conditions. A significant surface warming also occurs over the Pacific ocean east of Japan, which is caused by a weakening of offshore continental winds over Eastern Russia. Like today, warm and dry conditions prevail during El Niño over Australia and South Africa. However, a large increase in precipitation occurs over eastern Brazil at the LGM that is not observed during modern El Niño. This result is consistent with proxy evidence from this region indicating anomalously wet conditions at the LGM (Wang *et al.*, 2004). The symmetric equatorial Rossby wave response observed today (180E - 90W) is not as clearly evident in the 200 hPa streamfunction at the LGM.

Changes in winter sea surface temperature (SST) and polar sea ice during El Niño at the LGM are shown in Figure 2.7. Boreal winter SSTs increase most dramatically in the ocean surrounding Japan, in response to the overlying atmospheric warming associated with the weakening of offshore continental winds. A localized SST depression of 0.5 °C develops east of Greenland due to the retreat of sea ice in this region during El Niño and consequent exposure of surface waters to cold Arctic winds. Furthermore, a reduction of offshore ocean surface currents along the northern coast of South America and the eastern coast of Florida causes a local decrease in upwelling and hence warming at the

ocean surface.

Considerable changes in LGM winter sea ice margins are also evident at the poles during El Niño (Figure 2.7b). Near Antarctica, a thin filament of sea ice melts during El Niño to the east of the Ross ice shelf. An analogous sea ice reduction occurs along the eastern coast of Greenland. Significant melting of sea ice also occurs at lower latitudes, between Japan and mainland China and between the Aleutian islands and Russia, where localized LGM sea ice shelves decrease by one third their area during El Niño. Peak reduction of sea ice occurs beneath the large atmospheric warm anomaly over the southern portion of a thick sheet of polar sea ice off the coast of northeastern Russia; sea ice thins here by 0.5 to 1 m (approximately 25% of climatological DJF thickness) during El Niño at the LGM. In contrast, net sea ice thickening is apparent in the vicinity of Iceland and northeast Greenland, as well as off the coast of Antarctica, over the Ross ice shelf and in much of the Weddell Sea.

Regional climatological temperature and precipitation teleconnections over the Laurentide ice sheet at the LGM are depicted for El Niño and La Niña conditions in Figures 2.3 and 2.4, respectively, with surface wind vectors superimposed to highlight the underlying dynamics.

During El Niño (Figure 2.3), a large scale atmospheric warming of 1 °C occurs over the northern margin of the Laurentide ice sheet, caused by an intensification of the northern branch of the split jet and a consequent increase in advection of warm, low latitude air. This warming causes a 20% reduction in winter sea ice thickness during El Niño where the northern branch of the split jet passes over Baffin bay at the LGM (cf. Figure 2.7). An anticyclonic flow pattern is visible in the wind anomalies over the ice sheet and this increases the advection of cool air onto the southeastern Laurentide ice sheet margin resulting in a 1 °C cooling over the southeastern quadrant of the ice sheet during El Niño. The intensification of the northern branch of the split jetstream also acts to increase orographic precipitation rates over the southern coast of Alaska (Figure 2.3b). In contrast, weakening of the southern branch of the jet reduces orographic precipitation along the western coast of the ice sheet and along much of the southern margin of the ice sheet. Precipitation rates are

also enhanced during El Niño over the Baha peninsula and within the Atlantic storm track region, both areas in which El Niño temperature anomalies act to enhance the local atmospheric baroclinicity via changes in the meridional temperature gradient, particularly during the boreal winter months.

During La Niña (Figure 2.4) the northern branch of the split midlatitude jet stream weakens during the summer while the southern branch is intensified throughout the year. This results in anomalous cooling in the annual mean along the northern ice sheet margin due to a decrease in the advection of low latitude air by the northern jet branch. The intensification of the southern jet branch causes increased orographic precipitation along the western coast of California (0.1 mm/day to 0.2 mm/day) as well as onto the southeastern margin of the Laurentide ice sheet. Most of this precipitation occurs during the winter when the southern branch of the split jet is strongest. The enhancement of the southern jet also causes a localized warming of 0.8 °C over the southeastern ice sheet margin, not only by increasing the advection of low latitude air into this region but also by weakening the climatological anticyclonic flow pattern over the ice sheet. The thermal anomalies associated with La Niña conditions weaken the meridional temperature gradient in the vicinity of the southeastern ice margin and over the Atlantic storm tracks, reducing precipitation associated with baroclinic eddies in these areas.

#### **2.4.2 Effects of ENSO on the Laurentide Ice Sheet at the LGM**

The effects of ENSO teleconnections over North America on the growth and decay of the Laurentide ice sheet are discussed here. Results from the four 5000 year ice sheet simulations described in Section 2.3 (EN, LN, ENLN and ENLN-S) are depicted in Figures 2.8 to 2.10. Large scale changes are apparent in the final ice sheet thickness for each simulation due to regional mass balance adjustments near the ice margin that arise in response to forcing by the anomalous ENSO temperature and precipitation perturbations.

During El Niño conditions (Figure 2.8) the warming caused by the northern branch of the split jet stream greatly enhances ice ablation along the northern margin of the Laurentide ice sheet, increasing by a peak value of approxi-

mately 40 cm/a at the northwest margin. Prolonged exposure to this warm air anomaly over the course of the 5 kyr EN simulation resulted in a 50 m to 200 m thinning of ice along the entire northwest ice sheet margin and a localized reduction of ice where the jet crosses the southern coast of Alaska. An opposite effect occurred at the southeastern boundary of the ice sheet where cooler, wetter conditions reduced the ablation rate at the ice margin by as much as 30 cm/a in the EN simulation and caused a thickening of 50 m to 200 m relative to the control simulation.

Under persistent La Niña climatological forcing (Figure 2.9) large scale changes in the Laurentide ice sheet thickness are somewhat opposite to those simulated for the EN experiment near the ice sheet margins. Warming over the southeastern Laurentide (caused by the intensification of the southern jet stream branch during La Niña) resulted in a local ablation rate increase of 10 cm/a to 20 cm/a, which in turn caused an overall thinning of 50 m to 200 m near the southeastern ice sheet margin. At the northwest margin, exposure to cool atmospheric conditions during La Niña caused by the weakening of the summertime northern jet branch reduced the ablation rate by 10 cm/a to 20 cm/a, resulting in a modest thickening of 50 m to 100 m relative to the control run.

Due to the nonlinearity of the North American teleconnections associated with El Niño and La Niña, their combined effect on the dynamics of the Laurentide ice sheet at the LGM was nonzero. It is thus most logical to consider the long-term response of the ice sheet to averaged El Niño and La Niña climate anomalies. The combined El Niño / La Niña ice sheet simulation resulted in reduced ice thickness relative to control conditions along the northern ice sheet margin, where a thinning of 50 m to 100 m occurred, as well as off the southeastern coast of Baffin island, where ice thinned by as much as 200 to 300 m (Figure 2.10a). The former effect is due to the fact that the annually averaged warming of the northern jet branch during El Niño is higher in magnitude than the cooling during La Niña, resulting in a net positive ablation rate over the northwestern ice margin for the ENLN simulation. The latter effect arises as the warm EN anomaly positively reinforces anomalously warm

LN conditions in a region of reduced precipitation at the southeastern coast of Baffin island; the consequent increase in ice ablation and decrease in accumulation results in a strong localized net mass loss. In addition to these two thinning mechanisms, a modest ice gain of 30 m to 60 m also occurred at the southeast margin of the ice sheet, where the cold EN anomaly dominated LN warming and reduced the ablation rate.

The inclusion of seasonal variability in the ENSO climatological forcing fields significantly altered the ice sheet's dynamical response to ENLN climate forcing (Figure 2.10b). The interaction of the ENSO annual cycle with the seasonality of ice accumulation and ablation resulted in a reduced mass gain at the south east margin in comparison to the ENLN run. Furthermore, a large region of mass loss developed over the Great Lakes region and the ablation rate at the northwest margin was significantly reduced. Although several features of the non-seasonal ENLN run were consistent with the seasonal ENLN-S run (such as the localized mass loss anomaly over the southeastern coast of Baffin island) the net effect of including seasonal variations in the climate forcing was to reduce the Laurentide ice sheet's sensitivity to combined El Niño / La Niña climate forcing.

## 2.5 Conclusions

The GFDL AO-GCM simulation of ENSO at the LGM is characterized by modulations of the midlatitude split jet stream that cause strong extratropical teleconnections over North America relative to present-day conditions. When used to force a thermo-mechanic model of the Laurentide ice sheet on millennial time scales these teleconnections induce significant ice thickness adjustments near the ice sheet margins.

Variations in the intensity of the split midlatitude jetstream during El Niño and La Niña cause temperature and precipitation changes over North America that alter the regional mass balance of the Laurentide ice sheet, primarily at its north-western and south-eastern margins. During El Niño, the northern branch of the split jet stream intensifies and warms the northwestern ice sheet

margin; combined with a weakening of the southern jet stream branch this results in an intensification of the anticyclonic circulation pattern over the ice sheet interior that cools the southeastern margin. An opposite effect occurs in the LGM atmosphere during La Niña- the southernmost jetstream branch intensifies and the overlying anticyclone weakens. Under idealized persistent El Niño (La Niña) climate forcing the simulated response of the Laurentide ice sheet is thus a new equilibrium topographic state characterized by large scale thinning (thickening) at the northwest and thickening (thinning) at the southeast, of approximately 10%.

More realistic ice sheet simulations of the combined effects of El Niño and La Niña on the Laurentide ice sheet also produce ice thickness variability near the ice margins, due to the nonlinearity of the North American teleconnections. The equilibrium response of the ice sheet to an annually averaged ENSO perturbation is dominated by a weak El Niño-like signal (thinning at the northwest and thickening at the southeast). However, this response is sensitive to the seasonality of the ENSO cycle; the inclusion of annual cycle variability in the ENSO climate forcing results in an overall weaker thickness adjustment with additional thinning over the great lakes region.

It is clear from this study of the Laurentide ice sheet that climate variability at interannual timescales can have a significant effect on millennial scale cryospheric dynamics. The net influence of teleconnection patterns associated with the two phases of ENSO on low frequency ice dynamics is a spatially coherent climate forcing that results in a similarly well defined dynamical ice response. There remains much to learn about the role of other high frequency modes of oceanic and atmospheric variability in shaping the dynamical history of the Laurentide and other ice sheets in the Earth's past.

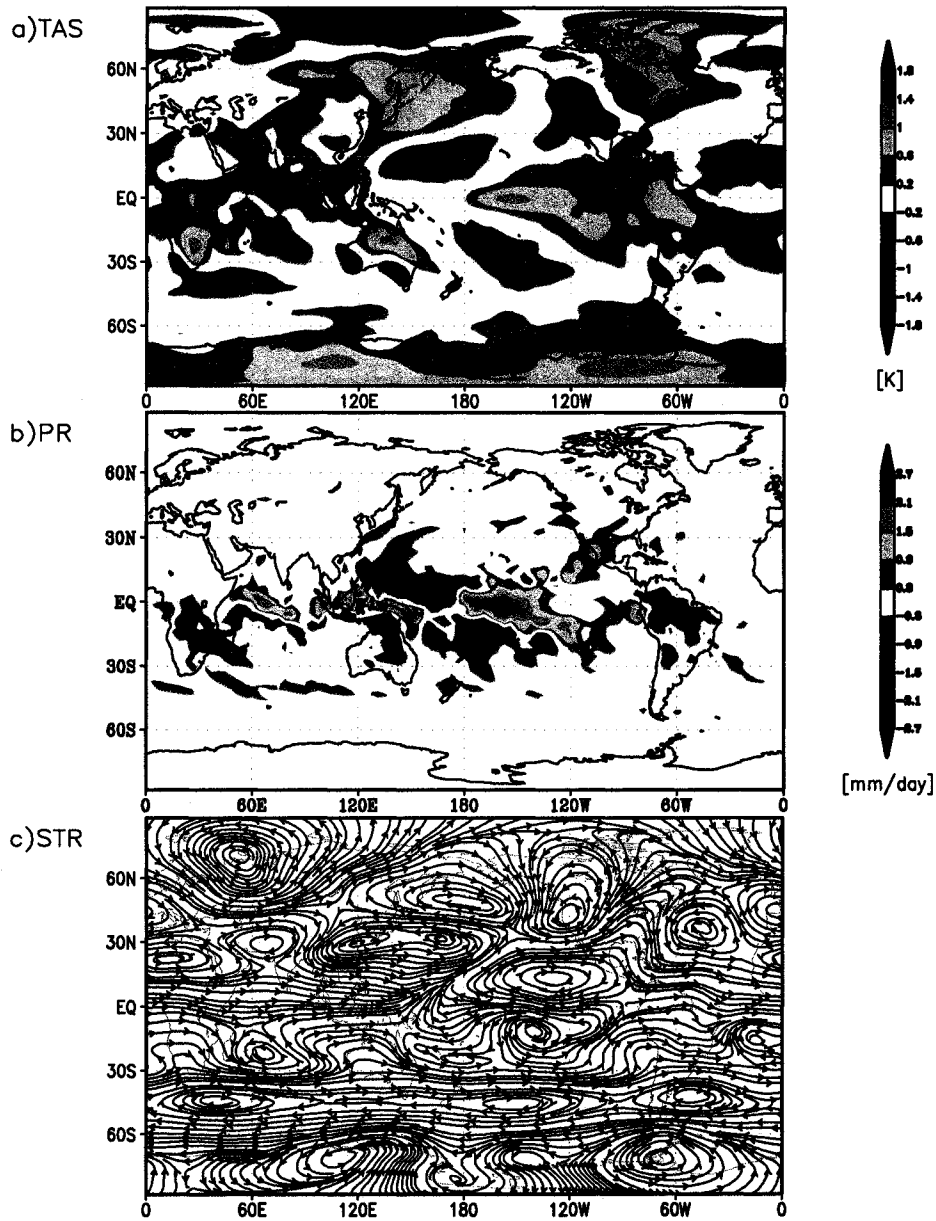
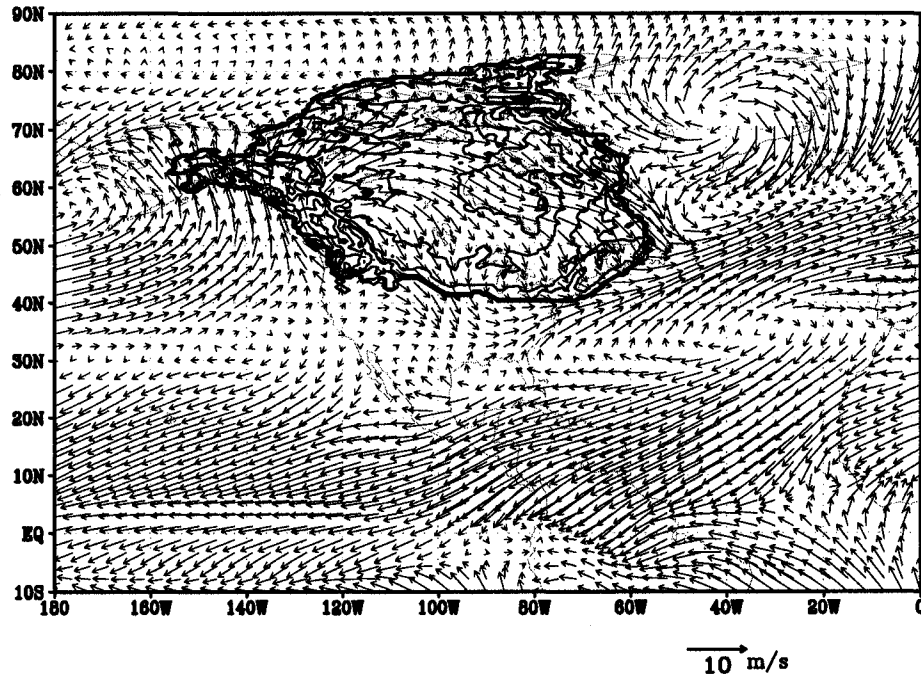


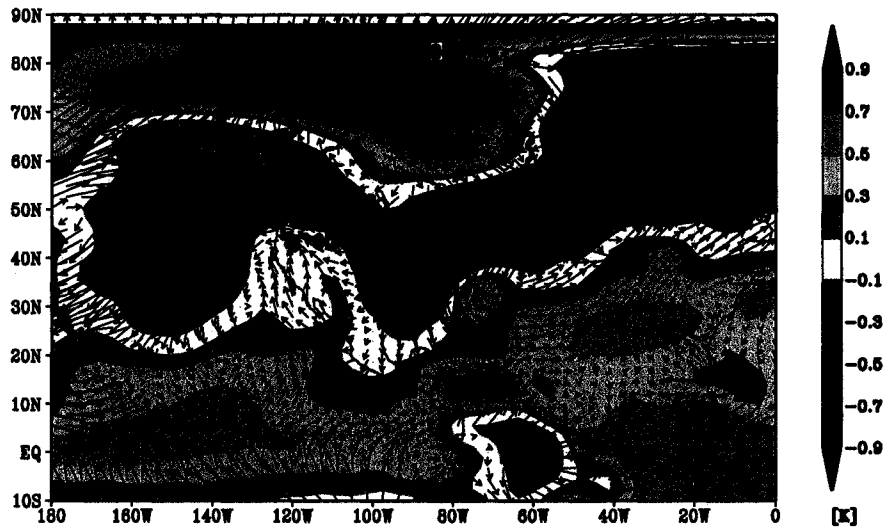
Figure 2.1: Global DJF El Niño anomalies as simulated by the GFDL AO-GCM for present-day conditions. El Niño climate perturbations are shown for a) the 30-m air temperature, b) precipitation and c) the 200 hPa stream function.



GrADS: COLA/IGES

Figure 2.2: Climatological 30-m winds over in the vicinity of the Laurentide ice sheet. The contours show Laurentide ice sheet topography.

a) TAS



b) PR

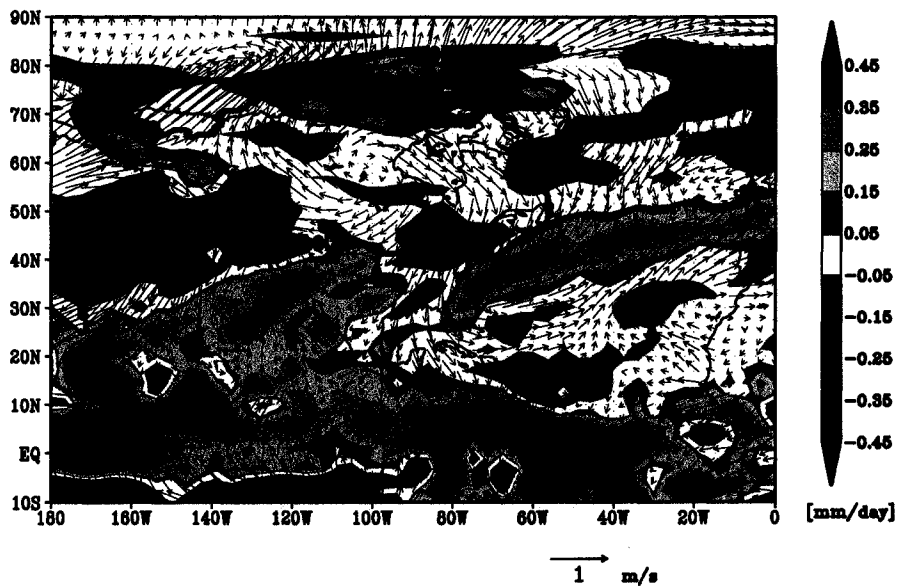


Figure 2.3: Annually averaged El Niño anomalies from the AO-GCM LGM climatology, shown over the Laurentide ice sheet for a) the 30-m air temperature and b) precipitation. The color scales shown only represent the range of variability over the ice sheet. These temperature and precipitation anomalies were used to drive the EN ice sheet simulation.

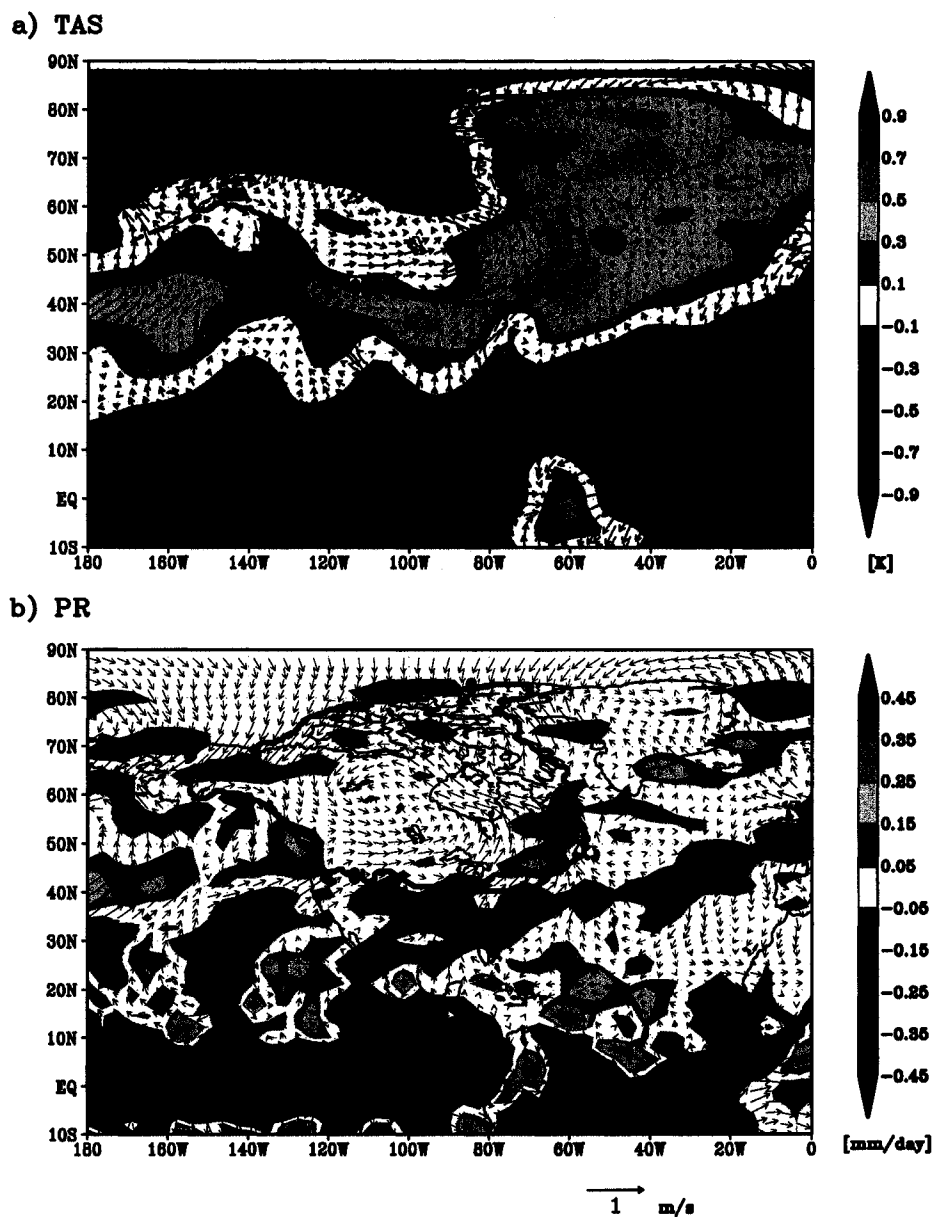


Figure 2.4: As in Figure 2.3, but for LGM La Niña conditions. These temperature and precipitation anomalies were used to drive the LN ice sheet simulation.

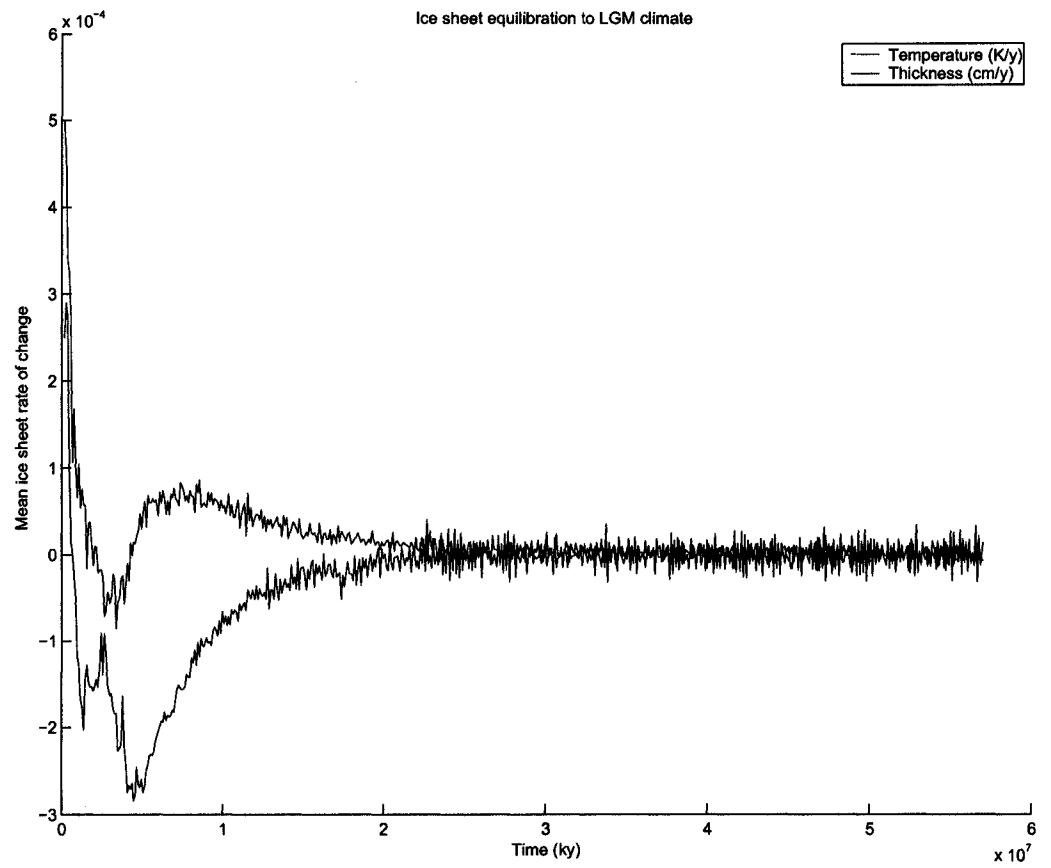


Figure 2.5: Temperature and thickness time series showing the equilibration of the Laurentide ice sheet to LGM climate simulated by an AO-GCM over a period of 57 kyr.

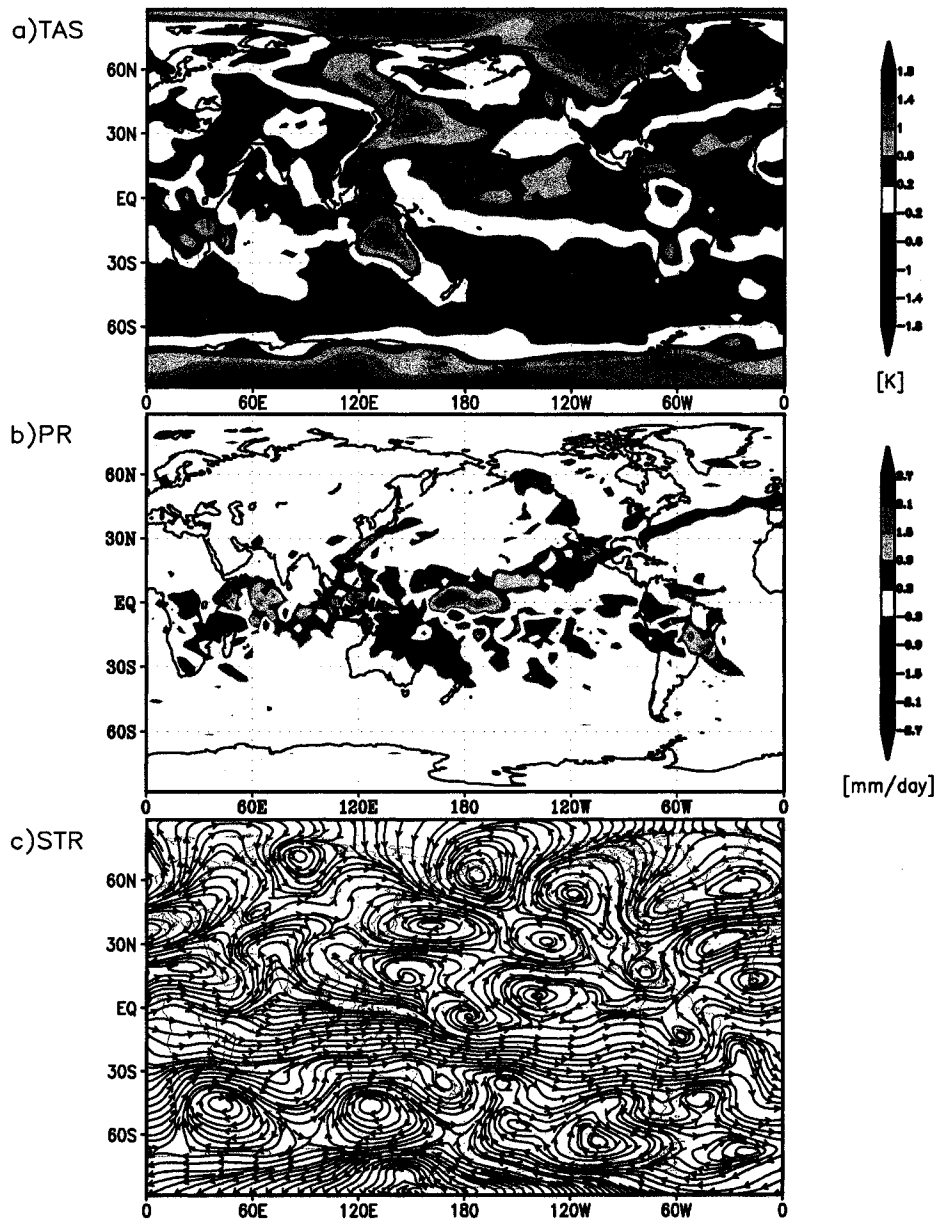
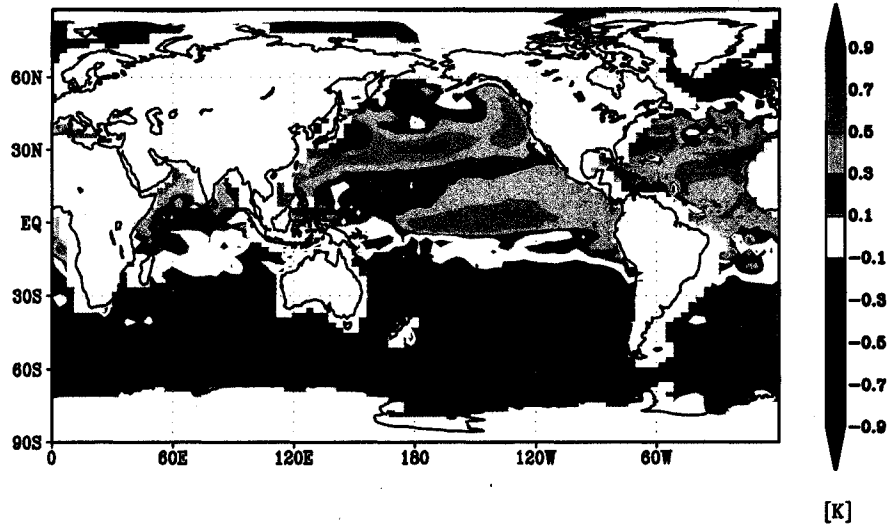


Figure 2.6: As in Figure 2.1, but for LGM El Niño conditions.

a) SST



b) SEA ICE

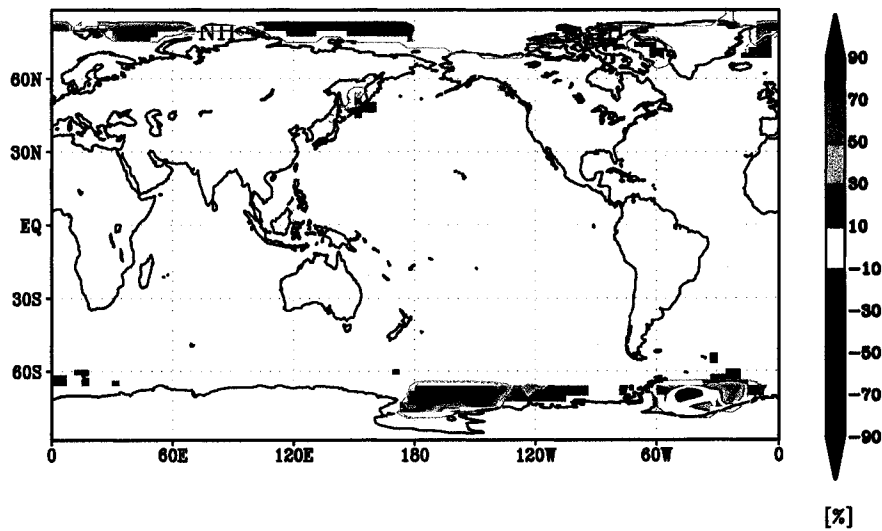


Figure 2.7: DJF El Niño anomalies of a) sea surface temperature and b) sea ice thickness for the AO-GCM LGM simulation. Sea ice margins for El Niño conditions are represented by the solid red contour, whilst the dashed contour depicts the climatological DJF sea ice margin.

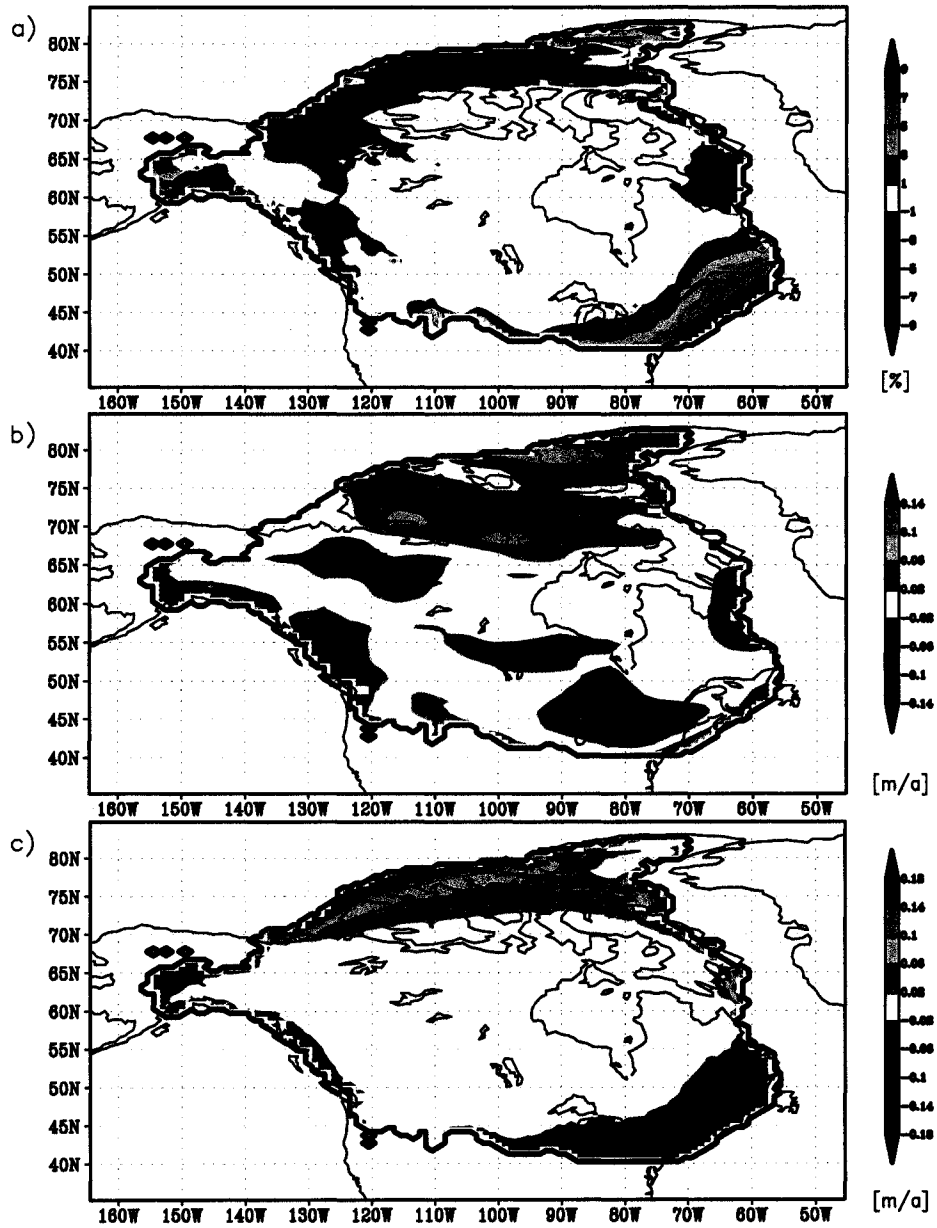


Figure 2.8: Laurentide ice sheet anomalies showing changes in a) final ice thickness, b) average ice accumulation and c) average ice ablation over the model domain for a 5 kyr simulation (EN) forced by El Niño-perturbed LGM climatology.

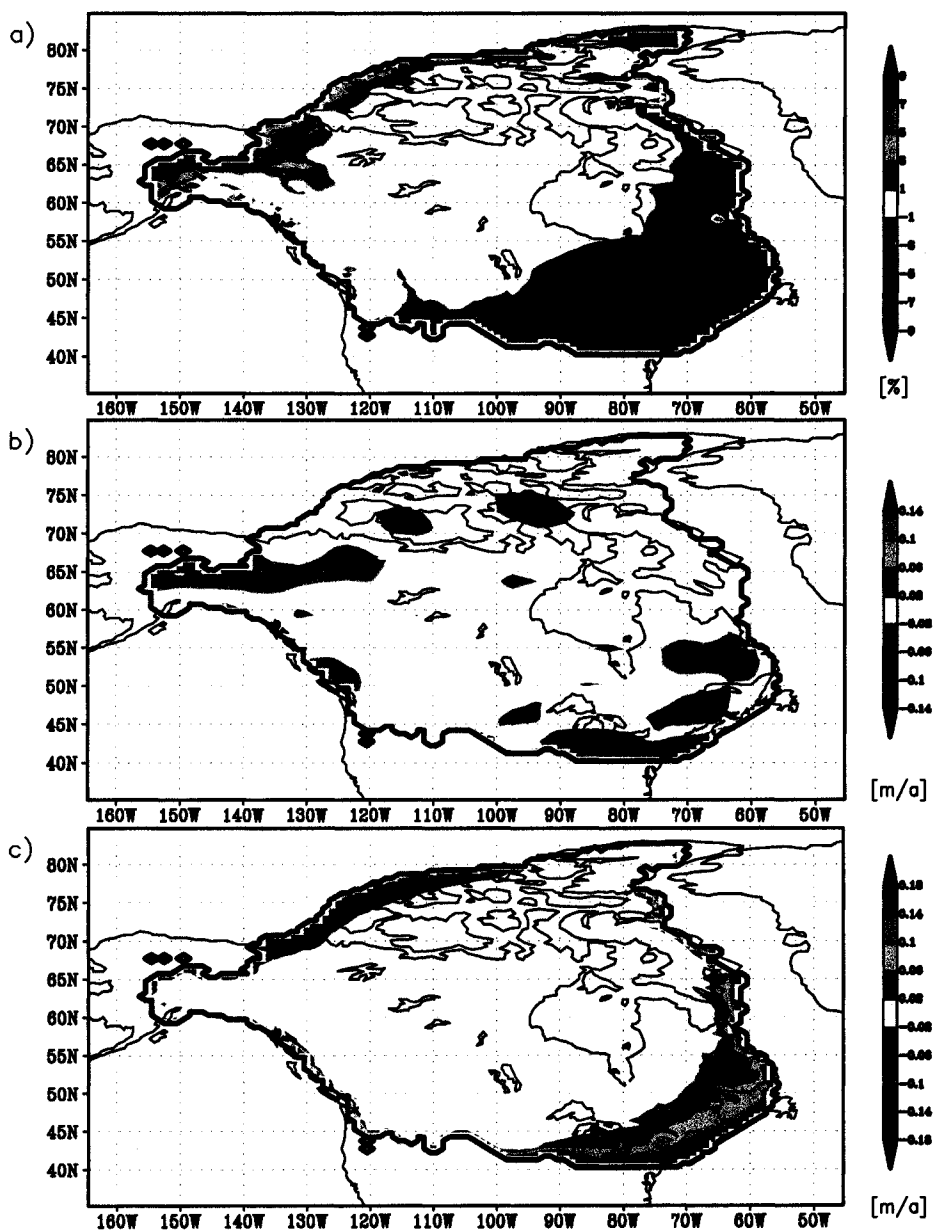
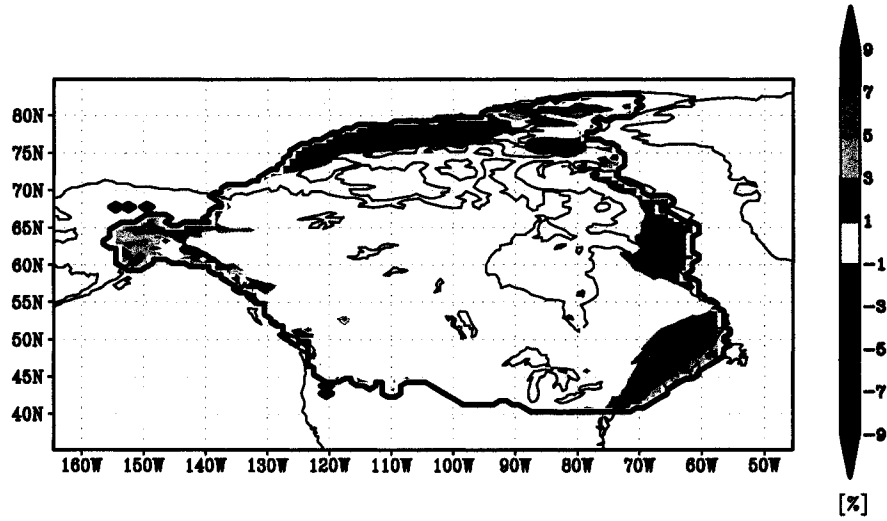


Figure 2.9: As in Figure 2.8, but for a 5 kyr simulation (LN) forced by La Niña-perturbed LGM climatology.

a)



b)

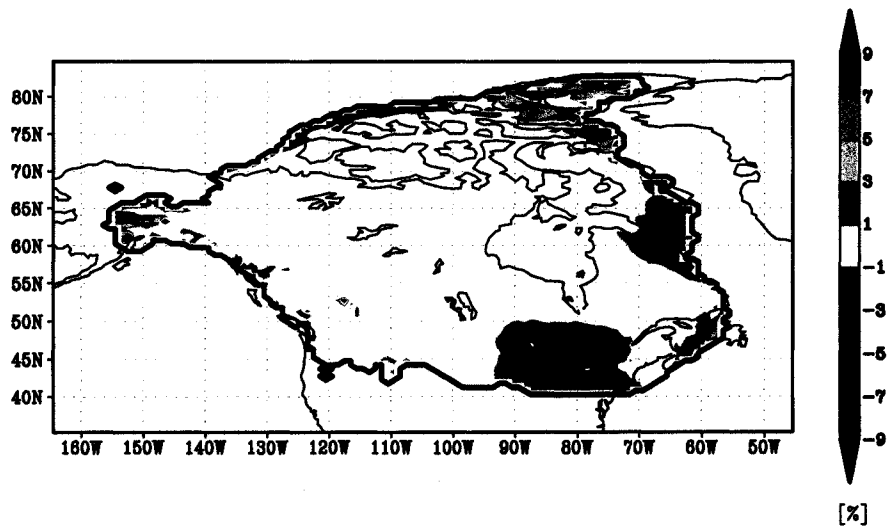


Figure 2.10: Laurentide ice sheet thickness anomalies showing changes in the final state due to combined El Niño and La Niña LGM climatological forcing for two 5 kyr ice sheet simulations. Figure 2.10a shows results from the ENLN simulation (in which ENSO seasonal variability was neglected), whereas Figure 2.10b is from the ENLN-S simulation, and retains monthly variability in the LGM ENSO signal.

# Bibliography

- AchutaRao, K., Sperber, K. R., 2002, "Simulation of the El Niño Southern Oscillation: Results from the Coupled Model Intercomparison Project", *Climate Dynamics*, **19**
- An, S. I., Wang, B., 2005, "The forced and intrinsic low-frequency modes in the North Pacific", *Journal of Climate*, **18**, 876–885
- Berger, W. H., von Rad, U., 2005, "Decadal to millennial cyclicity in varves and turbidites from the Arabian Sea: hypothesis of tidal origin", *Global and Planetary Change*, **34**, 313–325
- Braithwaite, R., 1984, "Calculation of degree-days for glacier-climate research", *Zeitschrift für Gletscherkunde und Glazialgeologie*, **20**, 1–8
- Bran, M., Hock, R., 2004, "Spatially distributed surface energy balance and ablation modelling on the ice cap of King George Island, Antarctica", *Global and Planetary Change*, **42**, 45–58
- Bryan, K., 1969, "A numerical method for the study of the circulation of the world ocean", *Journal of Computational Physics*, **3**, 347–376
- Bush, A. B. G., 2006, "Extra-tropical influence of the El Niño Southern Oscillation through the late Quaternary", *Journal of Climate*, *in press*
- Bush, Andrew B. G., Philander, S. George H., 1999, "The climate of the Last Glacial Maximum: Results from a coupled atmosphere-ocean general circulation model", *Journal of Geophysical Research*, **104**, 24 509–24 525
- DeWeaver, E., Nigam, S., 2004, "On the forcing of ENSO teleconnections by anomalous heating and cooling", *Journal of Climate*, **17**, 3225–3235
- Fanning, A. F., Weaver, A. J., 1996, "An atmospheric energy-moisture balance model: Climatology, interpentadal climate change, and coupling to an ocean general circulation model", *Journal of Geophysical Research*, **101**, 15 111–15 128
- Goosse, H., Renssen, H., 2004, "Exciting natural modes of variability by solar and volcanic forcing: idealized and realistic experiments", *Climate Dynamics*, **23**
- Gordon, C. T., Stern, W., 1982, "A description of the GFDL global spectral model", *Monthly Weather Review*, **110**, 625–644
- Hannachi, A., 2001, "Toward a nonlinear identification of the atmospheric response to ENSO", *Journal of Climate*, **14**, 2138–2149
- Huybrechts, P., 1990, "A 3-D model for the Antarctic ice sheet: a sensitivity study on the glacial-interglacial contrast", *Climate Dynamics*, **5**, 79–92

- Huybrechts, P., Gregory, J., Janssens, I., Wild, M., 2004, "Modelling Antarctic and Greenland volume changes during the 20th and 21st centuries forced by GCM time slice integrations", *Global and Planetary Change*, **42**, 83–105
- Jenssen, D., 1977, "A three-dimensional polar ice sheet model", *Journal of Glaciology*, **18**, 373–389
- Jöhannesson, T., Sigurdsson, O., Laumann, T., Kennett, M., 1995, "Degree-day glacier mass-balance modelling with application to glaciers in Iceland, Norway, and Greenland", *Journal of Glaciology*, **41**, 345–358
- Koutavas, A., Lynch-Stiaglitz, J., Marchitto, T. M., Sachs, J. P., 2002, "El Niño-like pattern in ice age tropical Pacific sea surface temperature", *Science*, **297**, 225–230
- Mahaffy, M. W., 1976, "A three-dimensional numerical model of ice sheets: tests on the Barnes Ice Cap, Northwest Territories.", *Journal of Geophysical Research*, **81**, 1059–1066
- Marshall, S. J., Clark, P. U., 2002, "Basal temperature evolution of North American ice sheets and implications for the 100-kyr cycle", *Geophysical Research Letters*, **29**, Art. No. 2214
- Marshall, S. J., Tarasov, L., Clarke, G. K. C., Peltier, W. R., 2000, "Glaciological reconstruction of the Laurentide ice sheet: physical processes and modelling challenges", *Canadian Journal of Earth Sciences*, **37**, 769–793
- Marshall, Shawn J., Clarke, G. K. C., 1997, "A continuum mixture model of ice stream thermomechanics in the Laurentide Ice Sheet: (1) Theory", *Journal of Geophysical Research - Solid Earth*, **102**, 20 599–20 613
- Marshall, Shawn J., James, Thomas S., Clarke, Garry K. C., 2002, "North American Ice Sheet Reconstructions at the Last Glacial Maximum", *Quaternary Science Reviews*, **21**, 175–192
- Newman, M., Compo, G. P., Alexander, M. A., 2003, "ENSO-forced variability of the Pacific decadal oscillation", *Journal of Climate*, **16**, 3853–3857
- Otto-Bliesner, B. L., Marshall, S. J., Overpeck, J. T., Miller, G. H., Hu, A., 2006, "Simulating Arctic climate warmth and icefield retreat in the last interglaciation", *Science*, **311**, 1751–1753
- Pacanowski, R. C., Philander, S. G. H., 1981, "Parameterization of vertical mixing in numerical models of tropical oceans", *Journal of Physical Oceanography*, **11**, 1443–1451
- Pacanowski, R. C., Dixon, K., Rosati, A., 1991, "The GFDL Modular Ocean Model user guide", *Tech. rep.*, Princeton, N. J.
- Peltier, W. R., 1985, "The LAGEOS constraint on deep mantle viscosity: results from a new normal mode method for the inversion of viscoelastic relaxation spectra", *Journal of Geophysical Research*, **90**, 9411–9421
- Philander, S. G., 1990, *El Niño, La Niña, and the Southern Oscillation*, Academic Press, San Diego
- Rasmusson, E. M., Carpenter, T. H., 1982, "Variations in tropical sea-surface temperature and surface wind fields associated with the Southern Oscillation El-Niño", *Monthly Weather Review*, **110**, 354–384

- Rosenthal, Y., Broccoli, A. J., 2004, "In Search of paleo-ENSO", *Science*, **304**, 219–221
- Sardeshmukh, P. D., Hoskins, B. J., 1988, "The Generation of Global Rotational Flow by Steady Idealized Tropical Divergence", *Journal of the Atmospheric Sciences*, **45**, 1228–1251
- Schneider, N., Comuelle, B. D., 2005, "The forcing of the Pacific decadal oscillation", *Journal of Climate*, **18**, 4355–4373
- Slonosky, V. C., Mysak, L. A., Derome, J., 1997, "Linking Arctic sea-ice and atmospheric circulation anomalies on interannual and decadal timescales", *Atmosphere-Ocean*, **35**, 333–366
- Stott, L., Poulsen, C., Lund, S., Thunell, R., 2002, "Super ENSO and global climate oscillations at millennial time scales", *Science*, **297**, 222–226
- Straus, D. M., Shukla, J., 2002, "Does ENSO force the PNA?", *Journal of Climate*, **15**, 2340–2358
- Trenberth, K. E., 1997, "The definition of El Niño", *Bulletin of the American Meteorological Society*, **78**, 2771–2777
- Trenberth, K. E., Caron, J. M., Stepaniak, D. P., Worley, S., 2002, "Evolution of El Niño-Southern Oscillation and global atmospheric surface temperatures", *Journal of Geophysical Research - Atmospheres*, **107**, Art. No. 4065
- Trombotto, D., Buk, E., Hernandez, J., 1997, "Monitoring of mountain permafrost in the Central Andes, Cordon del Plata, Mendoza, Argentina", *Permafrost and Periglacial Processes*, **8**, 123–129
- Tudhope, A. W., Chilcott, C. P., McCulloch, M. T., Cook, E. R., Chappell, J., Ellam, R. M., Lea, D. W., Lough, J. M., Shimmield, G. B., 2001, "Variability in the El Niño - Southern oscillation through a glacial-interglacial cycle", *Science*, **291**, 1511–1517
- van der Avoird, E., Dijkstra, H. A., Nauw, J. J., Schuurmans, C. J. E., 2002, "Nonlinearly induced low-frequency variability in a midlatitude coupled ocean-atmosphere model of intermediate complexity", *Climate Dynamics*, **19**, 303–320
- Wang, X., Auler, A. S., Edwards, R. L., Cheng, H., Cristaili, P. S., Smart, P. L., Richards, D. A., Shen, C.-C., 2004, "Wet periods in northeastern Brazil over the past 210 kyr linked to distant climate anomalies", *nature*, **432**, 740–743
- Wu, A., Hsieh, W. W., 2004, "The nonlinear patterns of North American winter temperature and precipitation associated with ENSO", *Journal of Climate*, **18**, 1736–1752
- Wu, P., Peltier, W. R., 1982, "Viscous gravitational relaxation", *Geophysical Journal of the Royal Astronomical Society*, **70**, 435–485
- Yin, J. H., Battisti, D. S., 2001, "The importance of tropical sea surface temperature patterns in simulations of last glacial maximum climate", *Journal of Climate*, **14**, 565–581

## Chapter 3

# Interactive atmosphere-ice coupling

### 3.1 Introduction

Dynamic and thermodynamic interactions between our atmosphere and continental ice sheets have the potential to generate climate variability on centennial to millennial timescales (e.g. Crowley, 1984; Crowley and North, 1990; Roe and Lindzen, 2001). For example, the areal extent and shape of an ice sheet determine both how much radiation is absorbed by the atmosphere and where precipitation occurs, which in turn alters the shape of the ice sheet. Understanding these types of interactions and the timescales involved is a crucial step towards understanding climate variability not only in the future (evolution of the Greenland and Antarctic ice sheets) but also in the past (evolution and migration of massive North American ice sheets over the past 900,000 years).

The interaction of ice sheets with the atmosphere is a difficult modeling topic that requires substantial computational resources to investigate. Until now, no theory or numerical tool existed that could address the full dynamic and thermodynamic coupling of these two components of the climate system on millennial timescales. Since ice sheet flows are orders of magnitude slower than atmospheric motions, continental ice is usually represented in climate simulations as a static boundary condition within an atmospheric general circulation model (AGCM) (e.g. Bromwich *et al.*, 2004; Lunt *et al.*, 2004; Kim, 2004; Shinn and Barron, 1989; Huybrechts *et al.*, 2002, 2004). Likewise, ice

sheet models (ISMs) are typically driven by uncoupled temperature and precipitation fields derived from GCM experiments or proxy data (e.g. Parizek and Alley, 2004; Forsstrom *et al.*, 2003; Forsstrom and Greve, 2004; Huybrechts *et al.*, 2004). The only atmospheric feedback built into this “one-way” climate coupling scheme is an approximation of the lapse rate effect, whereby climatological air temperatures are vertically interpolated along a constant atmospheric lapse rate to account for thermal adjustments associated with changes in the height of the ice sheet surface. Although the atmospheric lapse rate feedback has proven instrumental in simulating both modern ice sheets and ice sheets in the earth’s past (e.g. Marshall *et al.*, 2002; Huybrechts *et al.*, 2004), important dynamic and radiative ice-atmosphere interactions are not at all represented in this conventional one-way climate forcing scheme.

Fully interactive “two-way” coupling is the only way to simulate radiative and dynamic interactions between ice sheets and the atmosphere in a numerical modeling context. However, the development of interactively coupled ice sheet model (ISM)-AGCMs has been hindered by the disparity in timescales of the two fluids. Although this problem can be circumvented on millennial time scales through the use of an asynchronous ISM-AGCM coupling scheme, at the time of this writing only one attempt had been made to do so, in the context of a future climate simulation of the Greenland ice sheet (Ridley *et al.*, 2005). This study demonstrated the importance of resolving dynamic ice sheet-atmosphere feedbacks for millennial scale simulations of the Greenland ice sheet through the discovery of a dynamic atmospheric feedback that can act to stabilize the retreat of ice sheet margins.

It is likely that the influence of these sorts of feedback processes becomes more significant with increasing timescale, yet the effect of AGCM-ISM coupling on the 10 kyr scale evolution of ice sheets in the Earth’s past remains an open question. We address this issue in the present work, through the development of an asynchronous ISM-AGCM coupling scheme that is integrable on millennial timescales.

There is particular reason to believe that radiative atmosphere-ice feedbacks played an especially important role during the retreat of the Laurentide

ice sheet. Observations from Greenland indicate that relatively low surface albedos tend to develop in the ice ablation zone during the summer melt season (Knap and Oerlemans, 1996; Greuell and Knap, 2000). It is plausible that a similar seasonal ice albedo modulation took place in the massive ablation zones of the Laurentide ice sheet during its retreat, amplifying the influence of radiative feedbacks with the overlying atmosphere in these regions. Our AGCM-ISM coupling scheme accounts for this effect by incorporating a seasonal ice albedo parameterization in place of the standard constant-albedo representation of ice sheets in AGCMs.

We first test the fidelity of a new millennial-scale AGCM-ISM asynchronous coupling scheme that uses a melt-based parameterization of seasonal ice sheet albedo against both conventional one-way offline ISM climate forcing and against an AGCM-ISM coupling scheme that uses constant ice albedos. An overview of the numerical models, the coupling scheme as well as the seasonal ice albedo parameterization that we employ is presented in Section 3.2, and a detailed description of our simulations is provided in Section 3.3. The performance of our coupled model is evaluated in Section 3.4 by analyzing the melt response of a simulated Laurentide ice sheet to idealistically warm atmospheric conditions. Several conclusions are summarized in Section 3.5.

## 3.2 Model Description

### 3.2.1 Atmospheric Model

The atmospheric general circulation model that we employ is the Community Atmosphere Model v3.0 (CAM3) described in Collins *et al.* (2006), which is the working atmospheric component of the latest version of the Community Climate System Model developed at the National Center for Atmospheric Research in Boulder, CO. The model is a spectral primitive-equation AGCM, which we run at T31 resolution ( $3.7^\circ$  lat  $\times$   $3.75^\circ$  lon) with 25 vertical hybrid sigma levels. Orbital parameters and greenhouse gas mixing ratios for CO<sub>2</sub>, CH<sub>4</sub> and N<sub>2</sub>O are configurable during the model initialization; present-day values were taken from Collins and Rasch (2004) and LGM values from Pe-

tit *et al.* (1999). The AGCM is interactively coupled with the Community Land Model (CLM) (Bonan *et al.*, 2002), which handles subgrid land surface hydrology and radiative calculations for the CAM3 grid by subdividing each cell into a combination of five differentially treated land surface types (glacier, lake, wetland, urban and vegetated).

### 3.2.2 Ice Sheet Model

The ice sheet model used in this study is the 3-D thermo-mechanic model of Marshall and Clarke (1997), with ice dynamics based on Jenssen (1977) and thermodynamics following Mahaffy (1976). We employ this model to represent the Laurentide Ice Sheet on a North American domain with a longitudinal resolution of  $1^\circ$  and a latitudinal resolution of  $0.5^\circ$ . There are 20 vertical levels.

Ice flows according to viscous creep rheology governed by Glen’s flow law with an exponent of  $n = 3$  (Glen, 1958) and is subject to a sliding condition for the basal velocity whereby friction is relaxed when the pressure melting point at the base of the ice sheet is attained (Marshall *et al.*, 2002), viz:

$$v_b(\lambda, \theta, t) = -A_0 \alpha_T(\lambda, \theta, t) \rho_I g H \frac{\partial h_s}{\partial \chi} \quad (3.1)$$

where  $\lambda$  denotes longitude,  $\theta$  denotes latitude,  $v_b$  is the basal velocity,  $H$  is the ice thickness,  $g$  is the gravitational constant,  $\rho_I$  is the density of ice and  $h_s$  is the ice sheet surface height. Under this treatment, basal flow is enabled subject to a binary thermal switch  $\alpha_T$  which is activated provided ice is warm-based and local basal meltwater is available. The prescribed sliding rate is proportional to the local shear-stress following Payne (1998), and its magnitude is controlled by the model parameter  $A_0$ , which we fix at a value of  $0.008 \text{ m yr}^{-1} \text{ Pa}^{-1}$  (as in Marshall *et al.*, 2002). Basal topography responds to the evolving ice load on a mantle deformation timescale of 3000 yr through interactive coupling to an isostatic mantle-lithosphere based on Wu and Peltier (1982) and Peltier (1985).

It is prudent to note that uncertainties abound in the sub-grid scale representation of marine iceberg calving, basal hydrology, fast-flow ice stream-

ing and other processes involving longitudinal stresses (Marshall *et al.*, 2000). However, this shortcoming is merely representative of the current state of the art in ice sheet modeling, and an overall lack of understanding in the community on the appropriate model variables that control these processes. The Marshall and Clarke model has attained recognition in reconstructions of the topography of the Laurentide ice sheet at the LGM (Marshall *et al.*, 2002) as well as studies of the possible fate of the Greenland ice sheet (Otto-Bliesner *et al.*, 2006).

The primary control on ice sheet mass balance in the Marshall and Clarke ISM is a set of monthly climatological forcing maps of precipitation and air temperature imposed at the ice sheet surface, which are downscaled from a GCM grid to the higher resolution ISM grid using bilinear interpolation. Ice sheet mass balance is calculated as the difference between precipitative accumulation and both surface and basal melting. Snow accumulation onto the ice sheet is derived from the total AGCM monthly ice-equivalent precipitation forcing. Surface melt is parameterized using a conventional “positive degree day” scheme following the methodology of Braithwaite (1984). Briefly, monthly mean air temperatures from the AGCM are vertically interpolated to the evolving ice surface height, assuming a constant atmospheric lapse rate of 6 °C/km, and are assumed to represent a Gaussian probability distribution with a standard deviation of 5 °C. The use of a lapse rate somewhat less than the free air moist rate is consistent with several degree-day glaciological modeling studies (e.g. Bran and Hock (2004), Jóhannesson *et al.* (1995), Trombotto *et al.* (1997)). The available monthly melt energy is taken to be proportional to the number of days with positive temperature at the ice sheet surface, as computed from the air temperature distribution. We employ a degree day melt conversion factor for snow of  $d_s = 3.39 \text{ mm yr}^{-1}\text{°C}^{-1}$  and for ice of  $d_I = 9.04 \text{ mm yr}^{-1}\text{°C}^{-1}$ . Refreezing of meltwater up to a threshold fraction of 0.6 is permitted. Melt energy is consumed first to eliminate the accumulated and refrozen snowpack, with any excess energy transferred into ablation of the ice sheet itself.

The ISM climate forcing approach described above ensures that the strong

annual cycle of ice accumulation and ablation are incorporated into the ISM mass balance calculations while also approximating the important lapse rate ice-atmosphere feedback, which modulates the surface air temperature environment as ice heights evolve. However, it is by design a one-way coupling scheme that is incapable of capturing other significant (e.g. radiative and dynamic) feedbacks that ought to occur between the ice sheet and atmosphere.

### 3.2.3 AGCM-ISM coupling scheme

Fully interactive ice-atmosphere coupling requires communication not only from the atmosphere to the ice sheet, but vice versa as well. An interactive coupling infrastructure was therefore developed to communicate the topographic and radiative characteristics of the Marshall and Clarke ISM model state to the CAM3. Ice sheet orographic forcing was implemented in the CAM3 by imposing a spectrally decomposed version of the high-resolution ice topography into the surface geopotential boundary condition, as well as by altering the subgrid orography over the ice sheet, which is used by the CAM3 gravity wave drag scheme. To further capture ice radiative feedbacks, the land-surface characteristics in the CLM model were modified by adjusting the T31 fractional glacier coverage and soil textures over all ice-covered portions of the higher resolution ISM domain.

Due to the disparity in timescale of ice flow with respect to atmospheric flow, an asynchronous coupling scheme was developed to link separate AGCM and ISM integrations over an interactive ice-atmosphere simulation (Figure 3.1). Atmospheric dynamics were equilibrated to an initial ice sheet state on a timescale of 20 years, which was chosen to sample the range of interannual variability observed in the globally averaged AGCM eddy kinetic energy time series (see Figure 3.2). After the atmospheric equilibration process, the climatological annual cycle from the AGCM run was used to drive 1 kyr of ice evolution. Although this dynamic ice timescale is arbitrary, it is acceptably smaller than the overall equilibration timescale of the ice sheet model, which is on the order of 10 kyr (Figure 2.5). The AGCM was re-equilibrated to the resultant ice sheet state and the process repeated with the AGCM and

ISM exchanging data every 1000 years until the end of the coupled simulation. This approach is directly analogous to asynchronous coupling schemes that are currently used in GCMs.

### 3.2.4 A seasonal ice albedo parameterization

The default radiative treatment for all glacier land types in the land surface component of the CAM3 is to assign a constant albedo of 0.85 over all ice-covered regions, which is on the upper end of observed ice sheet albedos and fails to capture the observed tendency for lower albedos in the moist marginal ice sheet ablation zones during the summer melt season. In order to address this inadequacy and improve the fidelity of the CAM3 radiative response to interactive ISM coupling we therefore present a new melt-based ice albedo parameterization that can be incorporated into our AGCM-ISM coupling infrastructure.

For a given month  $N$ , the accumulated snowpack  $S(N)$  at a location on the ice sheet surface is given by:

$$S(N) = \sum_{n=9}^{12} a(n) - m_s(n) + \sum_{n=1}^N a(n) - m_s(n) \quad (3.2)$$

where summations are over months,  $a(n)$  is the monthly snow accumulation and  $m_s(n)$  the monthly snow melt. The contribution to the snowpack from the preceding year is assumed to have taken place primarily between the months of September ( $n = 9$ ) to December ( $n = 12$ ).

For  $S > 0$ , we represent the darkening of the surface snowpack due to snow melt by the following albedo parameterization:

$$\alpha(N) = \max \begin{cases} \alpha_o \\ \alpha_f - \beta \sum_{n=1}^N m_s(n) \end{cases} \quad (3.3)$$

where  $\alpha_o = 0.4$  is the threshold albedo for old snow,  $\alpha_f = 0.85$  is the fresh snow albedo, and  $\beta = -0.5 \text{ m}^{-1}$  is a linear coefficient relating changes in surface albedo to cumulative snow melt. Upon complete melting of the snowpack ( $S = 0$ ), a threshold ice albedo of  $\alpha_i = 0.5$  is imposed.

Figure 3.3 depicts this ice albedo parameterization as a function of the cumulative annual snow melt  $\sum_{n=1}^N m_s(n)$ . In low melt regimes such as winter and the elevated ice sheet interior, the albedo remains quite high, close to the default CLM value. However, a darkening results from the very high cumulative snow melt in the marginal ablation zones during the summer melt season. Figure 3.4 demonstrates this effect during the transition from winter to summer in a representative ISM simulation of the Laurentide ice sheet that incorporates the above ice albedo parameterization. The development of a low-albedo fringe of moist, radiatively absorptive ice around the ice sheet perimeter is clearly evident as the snowpack melts. This representation is more consistent with ice albedo observations than the default treatment in the CLM (setting  $\alpha = 0.85$  over all glacier land surface types) and thus constitutes a significant improvement to our AGCM-ISM coupling scheme.

### 3.3 Description of simulations

The role of ice-atmosphere feedbacks during deglaciation is first explored in the context of two persistently warm atmospheric scenarios with fixed modern SSTs, chosen to optimize the likelihood of inducing a significant melt response in an ISM simulation of the Laurentide Ice Sheet. Based on simple energetic calculations, the excess radiative forcing over the Laurentide ice sheet in both atmospheric configurations should in theory lead to substantial ice melt, thereby providing a test of the ISM melt response.

The initial ice sheet state originated from a snapshot of the Laurentide ice sheet at the Last Glacial Maximum (LGM), obtained from the simulation of Marshall and Clark (2002) and equilibrated to the AO-GCM LGM climatology of Bush (2006) over the course of a 57 kyr spin-up simulation. Figures 3.5 and 3.6 depict the ice sheet thickness and flow speeds, respectively, that were used to initialize the ISM integrations. The initial ice sheet thickness peaks in a 3500 m dome over the Hudson's Bay region, with outward channelized flow reaching peak speeds of 400 m/yr in regions of topographically steered ice convergence.

The two primary sources of radiative heating with the capacity to drive deglaciation are atmospheric greenhouse gases and orbital variations. Our ice sheet simulations were designed to isolate the sensitivity of the ISM melt response to extrema in both of these sources of radiative heating. Simulation results are then interpreted in light of the known deglaciation timescale of the Laurentide ice sheet as inferred from the proxy record, which is on the order of 10 kyr (Dyke *et al.*, 2002). In the first warm atmospheric scenario (GHG), greenhouse gas concentrations ( $\text{CO}_2$  and  $\text{CH}_4$ ) were fixed at their present-day values, bracketing the upper limit of radiative greenhouse warming that has occurred since the Last Glacial Maximum. Modern orbital forcing parameters were imposed. In the second warm atmosphere scenario (INS), greenhouse gas concentrations were reduced to their (minimum) LGM values, while mid-high latitude insolation during the summer melt season was increased to its maximum value since the LGM by imposing orbital parameters from 10000 BP (at which point there was a local maximum in the 41 kyr obliquity cycle). The ISM evolution in response to both persistently warm atmospheric states was investigated using a conventional one-way climate forcing approach in two 10 kyr simulations, which we refer to as 1WAY-GHG and 1WAY-INS. Analysis of these two simulations provides a means to test not only the fidelity of the ISM melt response under offline climate forcing, but also its relative sensitivity to orbital vs. greenhouse gas extrema during the Last Deglaciation.

As outlined in Section 3.2.2, one-way climate forcing does not capture several important atmosphere-ice feedback mechanisms. The influence of radiative and dynamic ice-atmosphere feedbacks was therefore explored for the GHG warm atmospheric scenario by comparing the 1WAY-GHG ISM simulation described above to an analogous two-way interactively coupled ice-atmosphere integration (2WAY-GHG), which employed the asynchronous coupling scheme outlined in Section 3.2.3. This coupled ice-atmosphere run was further repeated in a final experiment dubbed 2WAY-GHG+ALB, in which the effect of incorporating the improved seasonal ice albedo parameterization presented in Section 3.2.4 into the two-way interactive AGCM-ISM coupling infrastructure was explored.

### 3.4 Results

Figure 3.7 depicts time series of ice volume and ice area for the two 10 kyr simulations of the Laurentide Ice Sheet that were driven by offline idealized warm atmospheric forcing fields (1WAY-GHG and 1WAY-INS). Contrary to our expectations based on energetics calculations, neither the persistently warm greenhouse gas-rich atmospheric scenario nor the persistently high summer insolation configuration resulted in substantial deglaciation over the course of the 10 kyr ice sheet simulation. Neither accumulation nor ablation rates changed appreciably as a result of the atmospheric forcing. The high summer insolation case caused a larger melt response ( $\Delta V = -10.1\%$ ) than the high greenhouse gas scenario ( $\Delta V = -0.9\%$ ). This suggests that continental ice sheets may have been more sensitive to changes in the Earth's orbit than to changes in greenhouse gas concentrations during a glacial cycle.

The unrealistically low ISM melt response in both the 1WAY-GHG and 1WAY-INS experiments indicates that atmospheric feedbacks unresolved by conventional one-way climate forcing are likely important factors in modeling glacial cycles. In Figure 3.8, time series are shown for ice volume and area evolution from 2WAY-GHG, an interactively coupled atmosphere-ice sheet simulation configured for the high greenhouse gas atmospheric scenario, and compared to their one-way coupled analog (1WAY-GHG). Although two-way interactive coupling resulted in a modest increase in the ISM melt response ( $\Delta V = -2.8\%$ ) with respect to the 1WAY-GHG simulation ( $\Delta V = -0.9\%$ ), the overall ice sheet melt was still implausibly low given the extreme nature of the atmospheric forcing.

We found the failure of the interactively coupled 2WAY-GHG simulation to produce substantial deglaciation on a realistic timescale to be attributed to its treatment of ice albedos. Using a constant value of 0.85 underestimates the influence of radiative feedbacks over all ice covered terrain in the land surface component of the CAM3 and does not capture the positive feedback associated with albedo modulations in the ablation zones.

Figure 3.9 demonstrates how this problem was resolved through the inclu-

sion of a seasonal ice albedo parameterization in the AGCM-ISM coupling infrastructure. In contrast to the 2WAY-GHG simulation, the Laurentide ice sheet volume decreased dramatically in the 2WAY-GHG+ALB integration, with complete deglaciation occurring within a realistic timeframe of 5 kyr. The incorporation of reduced marginal ice albedos during the ablation season in 2WAY-GHG+ALB amplifies positive ice-atmosphere radiative feedbacks as ice retreats, ultimately leading to a widespread ISM melt response that is consistent with the idealistically warm atmospheric configuration. This sort of ice-albedo feedback is evidently crucial for the simulation of a realistic melt response and fundamentally cannot be represented without the use of a two-way interactive AGCM-ISM coupling scheme.

### 3.5 Conclusions

The results of our ISM simulations using conventional offline (one-way) AGCM forcing led to unrealistic ice sheet evolution on millennial timescales in response to two idealistically warm atmospheric states. The ISM melt response of a simulated Laurentide ice sheet to both high-greenhouse gas and high-insolation atmospheric configurations was vastly underestimated in both cases, highlighting the inadequacy of one-way climate forcing in millennial scale ice sheet modeling.

An initial attempt to improve the ISM melt response using a novel two-way asynchronous AGCM-ISM coupling scheme failed in a similar manner; the melt response to high greenhouse gas atmospheric conditions was again severely underestimated when the models were allowed to communicate at 1 kyr intervals. However, a realistic melt response was ultimately achieved by incorporating a seasonal parameterization for ice albedos into the two-way coupling infrastructure (Figure 3.9). Due to the decrease of ice albedos in the ice sheet ablation zones during the summer melt season, this modification effectively amplifies the radiative atmosphere-ice feedback in the two-way AGCM-ISM coupling scheme, thereby facilitating the retreat of the ice sheet in response to warm atmospheric conditions. This two-way coupled feedback

is large enough to dominate the ice sheet response to both intense greenhouse gas and orbital external forcings under conventional one-way climate forcing.

The effect of including interactive ocean dynamics in the ice-atmosphere coupling scheme remains an important open question, as this could alter the ice sheet melt sensitivity to warm atmospheric configurations. Whereas we fix sea surface temperatures at their present-day values in all our simulations, an interactive oceanic model would provide an additional pathway for high-latitude radiative energy to be transferred to the ice sheet via air-sea interactions and marine ice shelf melt.

Ultimately, we conclude that it is not possible to achieve plausible deglaciation of the Laurentide ice sheet in response to idealized warm atmospheric states without the use of an interactive ice-atmosphere coupling scheme that adequately represents the radiative feedbacks associated with seasonal modulations of ice albedos near the ice sheet margin. This finding casts new light on previous ice modeling studies that employ one-way climate forcing and represents an important step forward in the ongoing development of fully interactive asynchronous climate coupling schemes capable of simulating ice sheet-atmosphere feedbacks on millennial timescales.

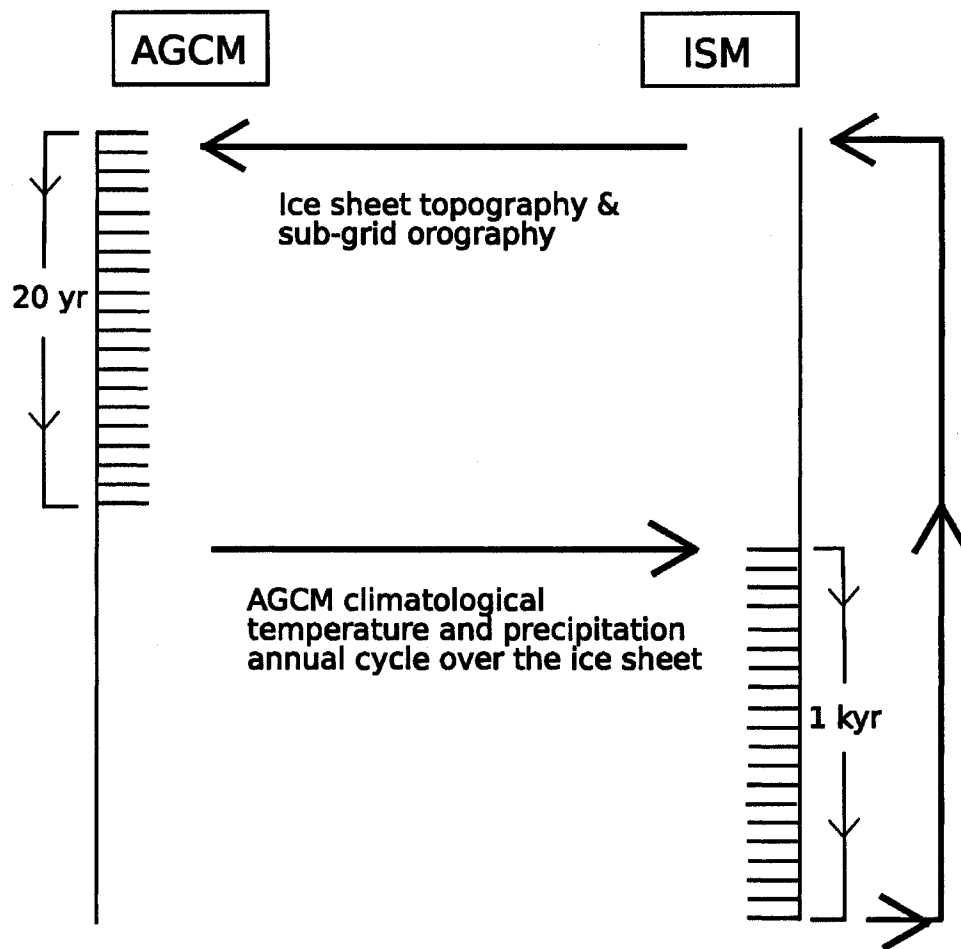


Figure 3.1: Schematic of the asynchronous ISM-AGCM coupling scheme. Atmospheric dynamics are equilibrated to a given ice sheet topography on a timescale of 20 years. The resultant climatological annual cycle of surface air temperature and precipitation are sent back to the ISM to drive the following 1000 years of ice evolution, and the process repeated.

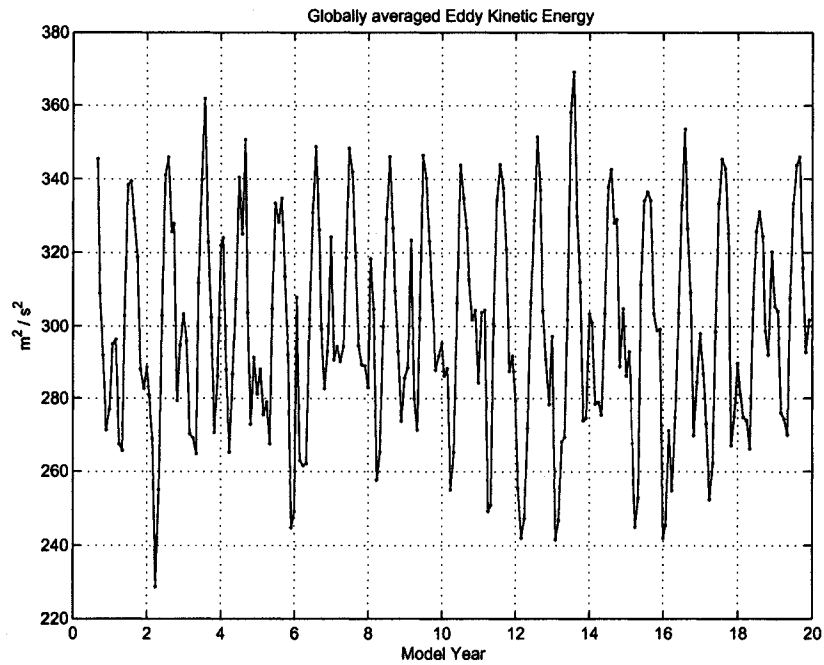


Figure 3.2: Time series of the monthly global-average eddy kinetic energy from a representative equilibration simulation of the Community Atmosphere Model v3.0 in response to an imposed Laurentide ice sheet topographic state. The choice of a 20 year atmospheric equilibration timescale is justified by the lack of an overall trend in this plot, and the demonstrated sampling of atmospheric interannual variability.

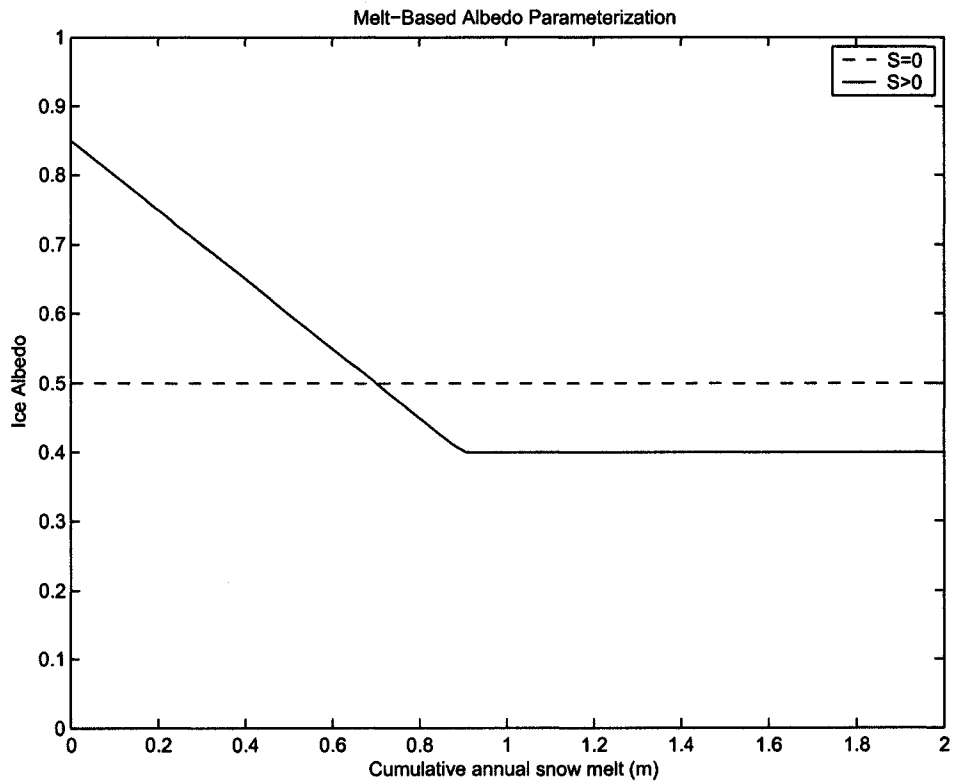


Figure 3.3: Ice albedo parameterization as a function of cumulative annual snowmelt. Regions of high snowpack melt (e.g. the summertime ablation zone) darken to a threshold of 0.4, whereas low melt regions (e.g. the ice sheet interior) remain snow-covered and reflective. A uniform ice albedo of 0.5 is imposed upon complete removal of the snowpack ( $S=0$ ). This scheme was incorporated into the 2WAY-GHG+ALB coupled simulation.

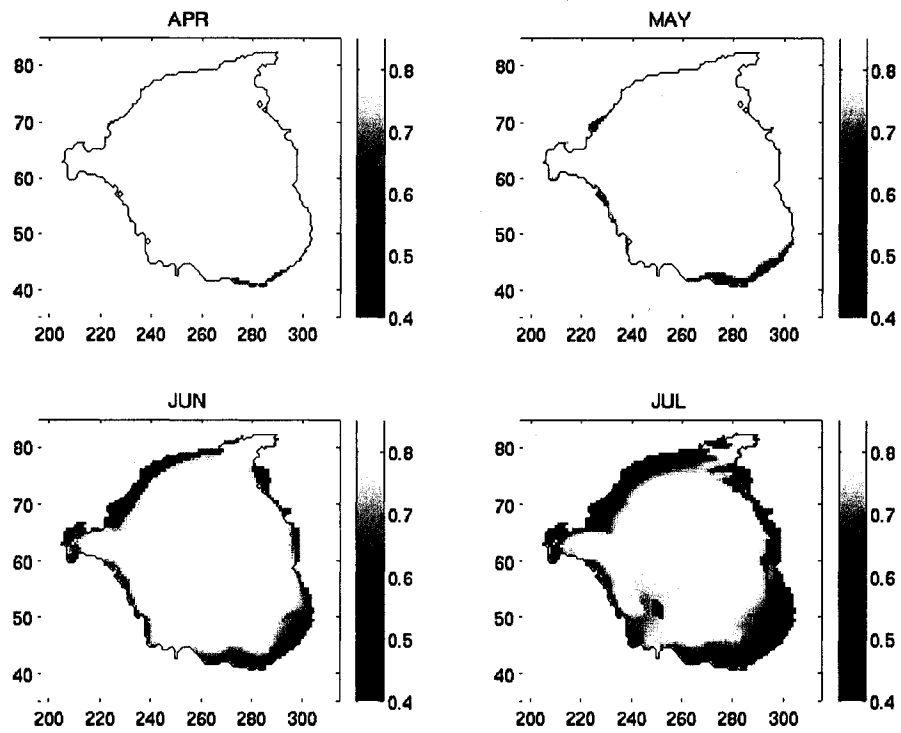


Figure 3.4: Monthly ice albedo maps computed during a representative ISM simulation of the Laurentide ice sheet that incorporates the new melt-based ice albedo parameterization depicted in Figure 3.3. The darkening of ice in the marginal ablation zone is clearly evident as the snowpack melts in this region during the transition to summer.

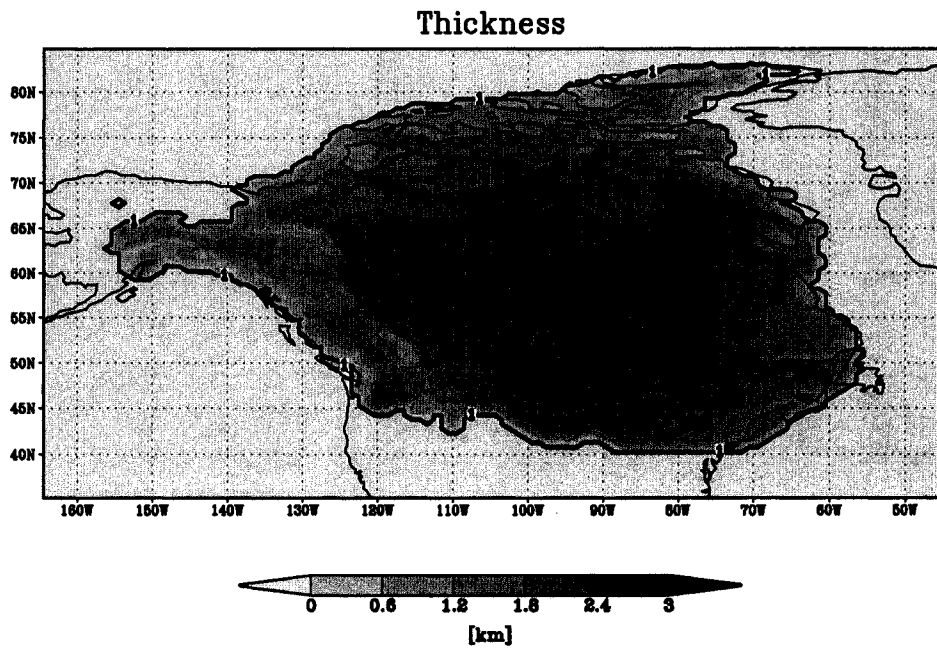


Figure 3.5: Initial ice thickness state of the Laurentide ice sheet, used to initialize the Marshall and Clarke ISM for all ice sheet simulations in the present study.

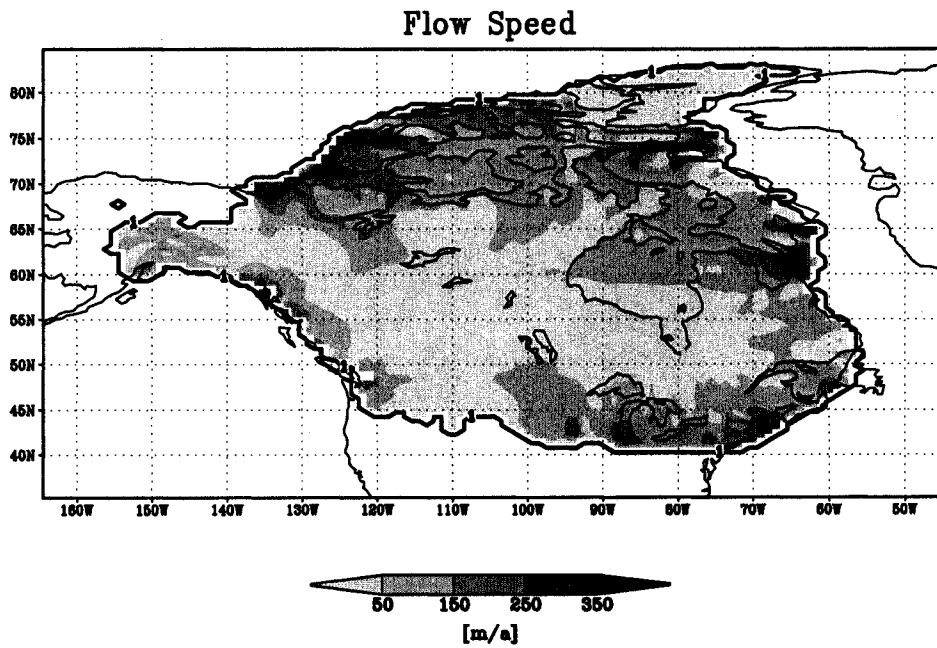


Figure 3.6: As in Figure 3.5, but for the initial ice flow state.

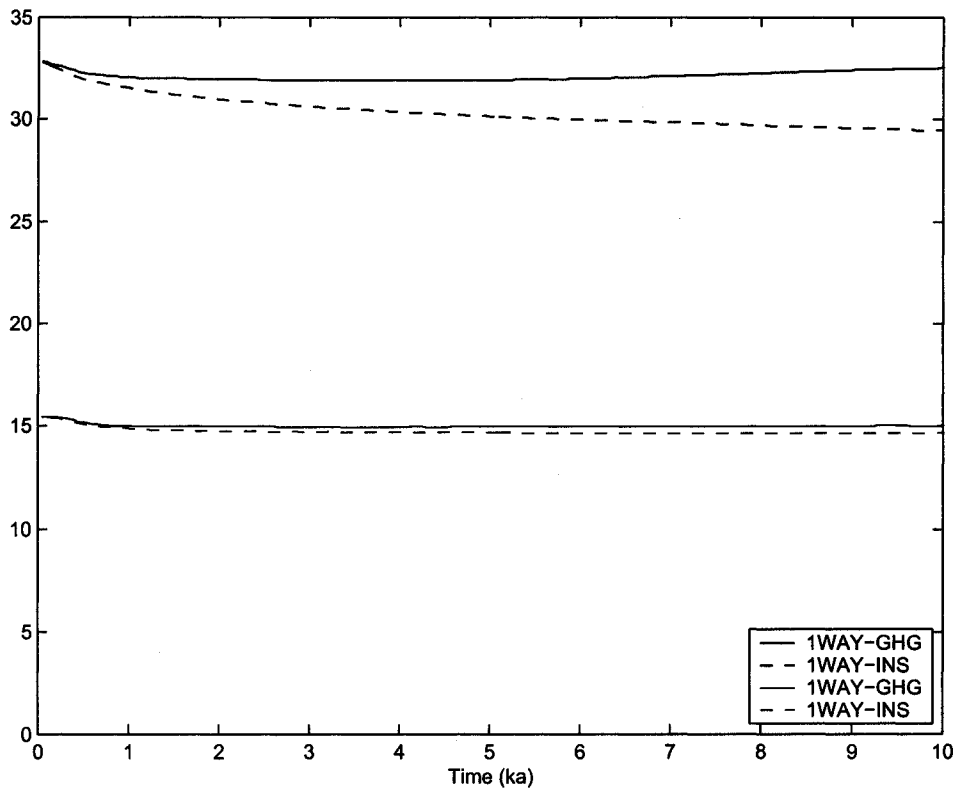


Figure 3.7: Volume (black lines;  $10^6 \text{ km}^3$ ) and area (blue lines;  $10^6 \text{ km}^2$ ) time series comparing the 1WAY-GHG (solid lines; high greenhouse gas, modern orbital parameters) and 1WAY-INS (dashed lines; low greenhouse gases, 10kyr BP maximum summer insolation) ice sheet simulations. Neither of the idealized warm atmosphere configurations produced appreciable melting under one-way climate forcing.

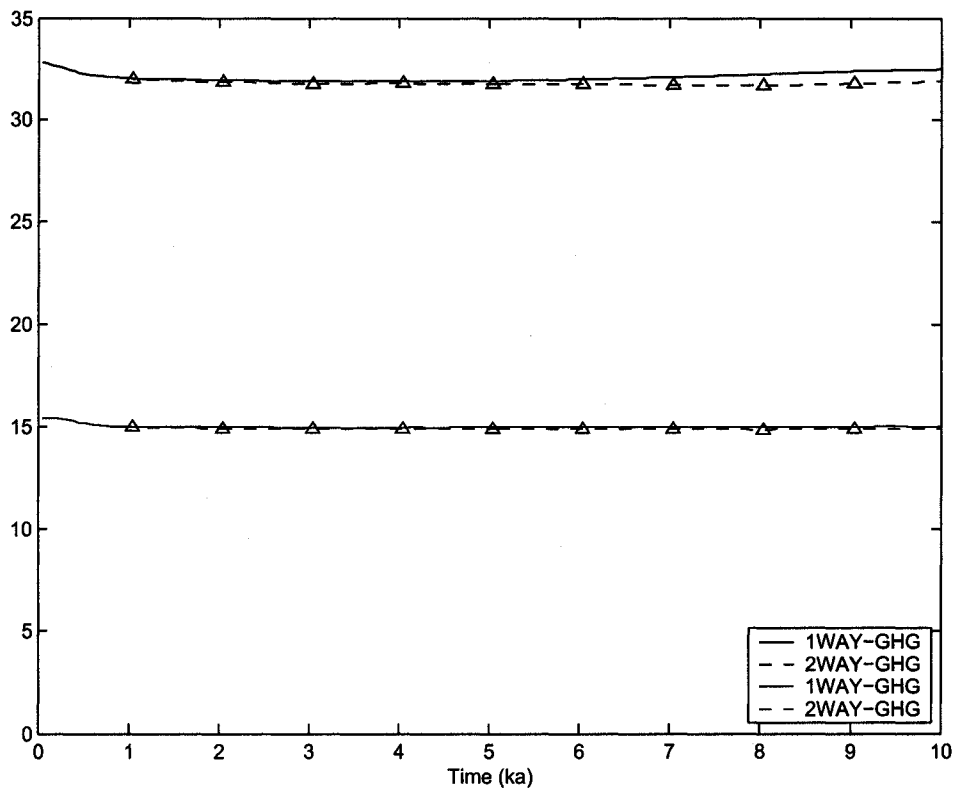


Figure 3.8: Volume (black lines;  $10^6 \text{ km}^3$ ) and area (blue lines;  $10^6 \text{ km}^2$ ) time series comparing the 1WAY-GHG (solid lines; high greenhouse gas, modern orbital parameters) and 2WAY-GHG (dashed lines; same configuration as 1WAY-GHG but with interactive ice-atmosphere coupling enabled) ice sheet simulations. Asynchronous ice-atmosphere coupling points in the 2WAY-GHG experiment are denoted by triangles. Inclusion of two-way ice-atmosphere coupling did not result in an increased melt response to the idealized high greenhouse gas warm atmospheric state.

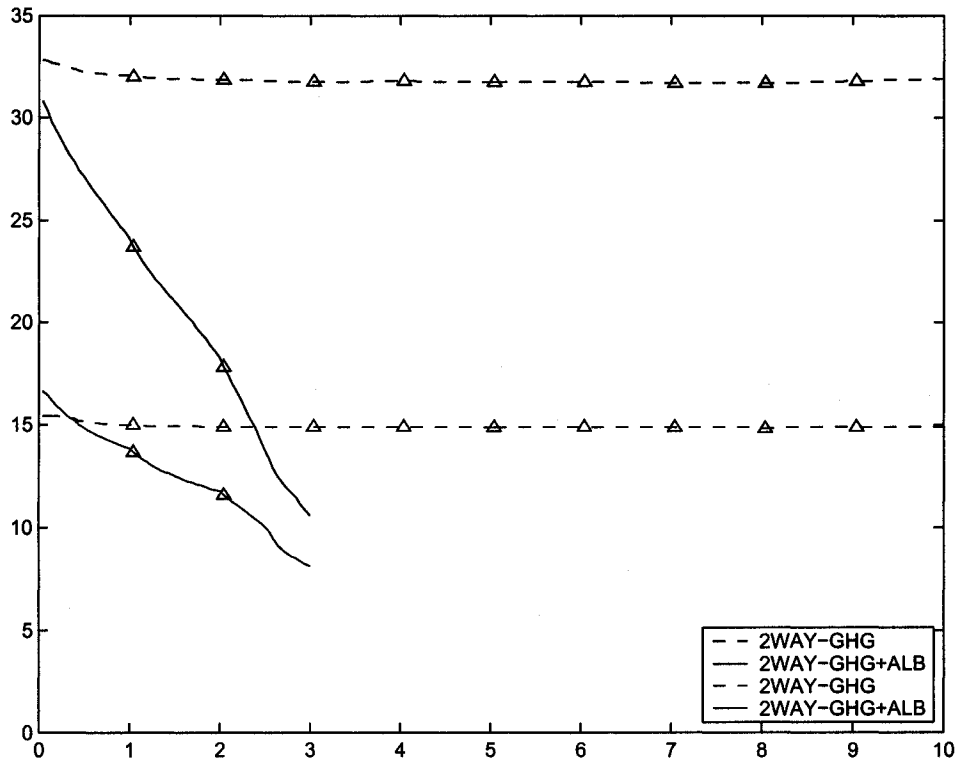


Figure 3.9: Volume (black lines;  $10^6 \text{ km}^3$ ) and area (blue lines;  $10^6 \text{ km}^2$ ) time series comparing the 2WAY-GHG (solid lines; uses an AGCM-ISM coupling scheme with constant ice albedos) to the 2WAY-GHG+ALB (dashed lines; uses an AGCM-ISM coupling scheme that incorporates a seasonal ice albedo parameterization). Asynchronous ice-atmosphere coupling points are denoted by triangles. The inclusion of a seasonal ice albedo parameterization in the coupling scheme results in the expected large ISM melt response to this idealistically warm atmospheric state. Due to computational and time constraints, the 2WAY-GHG+ALB run was executed for a significantly shorter time period than the 2WAY-GHG simulation.

# Bibliography

- Bonan, G. B., Oleson, K. W., Vertenstein, M., Levis, S., Zeng, X., Dai, Y., Dickinson, R. E., Yang, Z., 2002, "The land surface climatology of the Community Land Model coupled to the NCAR Community Climate Model", *Journal of Climate*, **15**, 3123–3149
- Braithwaite, R., 1984, "Calculation of degree-days for glacier-climate research", *Zeitschrift für Gletscherkunde und Glazialgeologie*, **20**, 1–8
- Bran, M., Hock, R., 2004, "Spatially distributed surface energy balance and ablation modelling on the ice cap of King George Island, Antarctica", *Global and Planetary Change*, **42**, 45–58
- Bromwich, David H., Toracinta, E. Richard, Wei, H., Oglesby, Robert J., Fastook, James L., Hughes, Terence J., 2004, "Polar MM5 simulation of the winter climate of the Laurentide ice sheet at the LGM", *Journal of Climate*, **17**, 3415–3433
- Bush, A. B. G., 2006, "Extra-tropical influence of the El Niño Southern Oscillation through the late Quaternary", *Journal of Climate*, *in press*
- Collins, W. D., Rasch, P. J., 2004, "Description of the NCAR Community Atmosphere Model (CAM 3.0)", *Tech. rep.*
- Collins, William D., Rasch, Philip J., Boville, Byron A., Hack, James J., McCaa, James R., Williamson, David L., Briegleb, Bruce P., Bitz, Cecilia M., Lin, Shian-Jiann, Zhang, Minghua, 2006, "The formulation and atmospheric simulation of the Community Atmosphere Model: CAM3", *Journal of Climate* (*in press*)
- Crowley, T. J., 1984, "Atmospheric circulation patterns during glacial inception - a possible candidate", *Quaternary Research*, **21**, 105–110
- Crowley, Thomas J., North, Gerald R., 1990, *Paleoclimatology*, Oxford University Press, Inc., New York
- Dyke, A. S., Andrews, J. T., Clark, P. U., England, J. H., Miller, G. H., Shaw, J., Veillette, J. J., 2002, "The Laurentide and Innuitian ice sheets during the Last Glacial Maximum", *Quaternary Science Reviews*, **21**, 9–31
- Forsstrom, P. L., Sallasmaa, O., Greve, R., Zwinger, T., 2003, "Simulation of fast-flow features of the Fennoscandian ice sheet during the Last Glacial Maximum", *Annals of Glaciology*, **37**, 383–389
- Forsstrom, Pirjo-Leena, Greve, Ralf, 2004, "Simulation of the Eurasian ice sheet dynamics during the last glaciation", *Global and Planetary Change*, **42**, 59–81

- Glen, J. W., 1958, "The flow law of ice: a discussion of the assumptions made in glacier theory, their experimental foundations and consequences", *International Association of Hydrological Sciences*, **47**, 171–183
- Greuell, W., Knap, W. H., 2000, "Remote sensing of the albedo and detection of the slush line on the Greenland ice sheet", *Journal of Geophysical Research - Atmospheres*, **105**, 15 567–15 576
- Huybrechts, P., Janssens, I., Pocin, C., Fichet, T., 2002, "The response of the Greenland ice sheet to climate changes in the 21st century by interactive coupling of an AOGCM with a thermomechanical ice-sheet model", *Annals of Glaciology*, **35**, 409–415
- Huybrechts, P., Gregory, J., Janssens, I., Wild, M., 2004, "Modelling Antarctic and Greenland volume changes during the 20th and 21st centuries forced by GCM time slice integrations", *Global and Planetary Change*, **42**, 83–105
- Jenssen, D., 1977, "A three-dimensional polar ice sheet model", *Journal of Glaciology*, **18**, 373–389
- Jøhannesson, T., Sigurdsson, O., Laumann, T., Kennett, M., 1995, "Degree-day glacier mass-balance modelling with application to glaciers in Iceland, Norway, and Greenland", *Journal of Glaciology*, **41**, 345–358
- Kim, S. J., 2004, "The effect of atmospheric CO<sub>2</sub> and ice sheet topography on LGM climate", *Climate Dynamics*, **22**, 639–651
- Knap, W. H., Oerlemans, J., 1996, "The surface albedo of the Greenland ice sheet: Satellite-derived and in situ measurements in the Sondre Stromfjord area during the 1991 melt season", *Journal of Glaciology*, **42**, 364–374
- Lunt, Daniel J., de Noblet-Ducoudr, Nathalie, Charbit, Sylvie, 2004, "Effects of a melted Greenland ice sheet on climate, vegetation, and the cryosphere", *Climate Dynamics*, **23**, 679–694
- Mahaffy, M. W., 1976, "A three-dimensional numerical model of ice sheets: tests on the Barnes Ice Cap, Northwest Territories.", *Journal of Geophysical Research*, **81**, 1059–1066
- Marshall, S. J., Clark, P. U., 2002, "Basal temperature evolution of North American ice sheets and implications for the 100-kyr cycle", *Geophysical Research Letters*, **29**, Art. No. 2214
- Marshall, S. J., Tarasov, L., Clarke, G. K. C., Peltier, W. R., 2000, "Glaciological reconstruction of the Laurentide ice sheet: physical processes and modelling challenges", *Canadian Journal of Earth Sciences*, **37**, 769–793
- Marshall, Shawn J., Clarke, G. K. C., 1997, "A continuum mixture model of ice stream thermomechanics in the Laurentide Ice Sheet: (1) Theory", *Journal of Geophysical Research - Solid Earth*, **102**, 20 599–20 613
- Marshall, Shawn J., James, Thomas S., Clarke, Garry K. C., 2002, "North American Ice Sheet Reconstructions at the Last Glacial Maximum", *Quaternary Science Reviews*, **21**, 175–192
- Otto-Bliesner, B. L., Marshall, S. J., Overpeck, J. T., Miller, G. H., Hu, A., 2006, "Simulating Arctic climate warmth and icefield retreat in the last interglaciation", *Science*, **311**, 1751–1753

- Parizek, Byron R., Alley, Richard B., 2004, "Implications of increased Greenland surface melt under global-warming scenarios: ice-sheet simulations", *Quaternary Science Reviews*, **23**, 1013–1027
- Payne, A. J., 1998, "Dynamics of the Siple Coast ice streams, West Antarctica: results from a thermomechanical ice sheet model", *Geophysical Research Letters*, **25**, 3173–3176
- Peltier, W. R., 1985, "The LAGEOS constraint on deep mantle viscosity: results from a new normal mode method for the inversion of viscoelastic relaxation spectra", *Journal of Geophysical Research*, **90**, 9411–9421
- Petit, J. R., Jouzel, J., Raynaud, D., Barkov, N. I., Barnola, J. M., Basile, I., Bender, M., Chappellaz, J., Davis, J., Delaygue, G., Delmotte, M., Kotlyakov, V. M., Legrand, M., Lipenkov, V., Lorius, C., Pepin, L., Ritz, C., Saltzman, E., Stievenard, M., 1999, "Climate and atmospheric history of the past 420,000 years from the Vostok ice core, Antarctica", *Nature*, **399**, 429–436
- Ridley, J. K., Huybrechts, P., Gregory, J. M., Lowe, J. A., 2005, "Elimination of the Greenland ice sheet in a high CO<sub>2</sub> climate", *Journal of Climate*, **18**, 3409–3427
- Roe, G. H., Lindzen, R. S., 2001, "The mutual interaction between continental-scale ice sheets and atmospheric stationary waves", *Journal of Climate*, **14**, 1450–1465
- Shinn, Richard A., Barron, Eric J., 1989, "Climate sensitivity to continental ice sheet size and configuration", *Journal of Climate*, **2**, 1517–1537
- Trombotto, D., Buk, E., Hernandez, J., 1997, "Monitoring of mountain permafrost in the Central Andes, Cordón del Plata, Mendoza, Argentina", *Permafrost and Periglacial Processes*, **8**, 123–129
- Wu, P., Peltier, W. R., 1982, "Viscous gravitational relaxation", *Geophysical Journal of the Royal Astronomical Society*, **70**, 435–485

## Chapter 4

# General Discussion and Conclusions

Both of the papers presented in this thesis constitute a significant contribution to the emerging field of coupled ice sheet-atmosphere modelling. In Chapter 2 we have demonstrated that modes of atmospheric variability at frequencies other than the annual cycle have the capacity to drive significant ice sheet thickness adjustments on millennial timescales. In Chapter 3, we show that the conventional modelling approach of forcing ISM simulations by offline climate data can lead to unphysical results under idealized atmospheric conditions. Both of these findings motivate a need to incorporate fully interactive asynchronous atmospheric coupling into ice sheet models. We implement the first such ice sheet-atmosphere coupling scheme in Chapter 3 and demonstrate that it offers significant improvements to the millennial-scale ISM response (Figure 3.9), provided a representation of seasonal ice albedo changes is included in the two-way coupling infrastructure.

The effects of interannual atmospheric ENSO variability at the Last Glacial Maximum on the millennial scale dynamics of the Laurentide ice sheet were explored in Chapter 2 via a series of ice sheet simulations forced by AO-GCM output. The nonlinearity of North American teleconnection patterns associated with El Niño and La Niña at the LGM results in a net atmospheric forcing over the ENSO cycle that acts as a persistent forcing on millennial scale ice sheet evolution. The LGM ENSO signature from the AO-GCM is characterized by strong high latitude teleconnections that include modulations of

the split jet stream structure, which have regional mass balance implications for the Laurentide ice sheet. Idealized ice sheet simulations driven by persistent El Niño (La Niña) climatological perturbations result in overall thinning (thickening) at the northwest margin of the Laurentide ice sheet on the order of 10% of the initial ice thickness, and vice versa at the southeastern margin. Ice sheet simulations forced by an averaged El Niño + La Niña teleconnection perturbation are dominated by the stronger El Niño response and are sensitive to the seasonality of the LGM ENSO cycle.

In Chapter 3, the role of ice sheet-atmosphere feedbacks during the Last Deglaciation was investigated on a millennial timescale via a series of coupled and uncoupled thermo-mechanic ice sheet model (ISM) simulations. We find that conventional one-way climate forcing of an ISM by atmospheric general circulation model (AGCM) output results in an unrealistically insensitive melt response to two idealized warm atmosphere configurations. The ISM melt response is greatly improved through the application of interactive two-way AGCM-ISM coupling and a new ice albedo parameterization that captures the increased radiative absorptivity of marginal ice during the summer melt season (Figure 3.9). This new two-way asynchronous coupling infrastructure is the first of its kind, and is a suitable tool to drive millennial-scale coupled ice-atmosphere simulations of continental deglaciation.

Our findings confirm the notion that dynamic and thermodynamic atmosphere-ice feedbacks played a significant role in the evolution of massive continental ice sheets in the Earth's past. We clearly demonstrate that both interannual- (Chapter 2) and millennial-scale (Chapter 3) atmospheric variability constitute a non-negligible forcing on long term ice sheet evolution, and that millennial-scale radiative feedbacks between the cryosphere and atmosphere require special treatment due to seasonal ice albedo changes. These results provide a foundation for future coupled atmosphere-ice sheet studies, and are an important first step towards the development of an Earth system model capable of resolving coupled climate-cryosphere dynamics on paleo-climatological timescales.

# Bibliography

- AchutaRao, K., Sperber, K. R., 2002, "Simulation of the El Niño Southern Oscillation: Results from the Coupled Model Intercomparison Project", *Climate Dynamics*, **19**
- An, S. I., Wang, B., 2005, "The forced and intrinsic low-frequency modes in the North Pacific", *Journal of Climate*, **18**, 876–885
- Berger, W. H., von Rad, U., 2005, "Decadal to millennial cyclicity in varves and turbidites from the Arabian Sea: hypothesis of tidal origin", *Global and Planetary Change*, **34**, 313–325
- Bonan, G. B., Oleson, K. W., Vertenstein, M., Levis, S., Zeng, X., Dai, Y., Dickinson, R. E., Yang, Z., 2002, "The land surface climatology of the Community Land Model coupled to the NCAR Community Climate Model", *Journal of Climate*, **15**, 3123–3149
- Braithwaite, R., 1984, "Calculation of degree-days for glacier-climate research", *Zeitschrift für Gletscherkunde und Glazialgeologie*, **20**, 1–8
- Bran, M., Hock, R., 2004, "Spatially distributed surface energy balance and ablation modelling on the ice cap of King George Island, Antarctica", *Global and Planetary Change*, **42**, 45–58
- Bromwich, David H., Toracinta, E. Richard, Wei, H., Oglesby, Robert J., Fastook, James L., Hughes, Terence J., 2004, "Polar MM5 simulation of the winter climate of the Laurentide ice sheet at the LGM", *Journal of Climate*, **17**, 3415–3433
- Bryan, K., 1969, "A numerical method for the study of the circulation of the world ocean", *Journal of Computational Physics*, **3**, 347–376
- Bush, A. B. G., 2006, "Extra-tropical influence of the El Niño Southern Oscillation through the late Quaternary", *Journal of Climate*, *in press*
- Bush, Andrew B. G., Philander, S. George H., 1999, "The climate of the Last Glacial Maximum: Results from a coupled atmosphere-ocean general circulation model", *Journal of Geophysical Research*, **104**, 24 509–24 525
- Collins, W. D., Rasch, P. J., 2004, "Description of the NCAR Community Atmosphere Model (CAM 3.0)", *Tech. rep.*
- Collins, William D., Rasch, Philip J., Boville, Byron A., Hack, James J., McCaa, James R., Williamson, David L., Briegleb, Bruce P., Bitz, Cecilia M., Lin, Shian-Jiann, Zhang, Minghua, 2006, "The formulation and atmospheric simulation of the Community Atmosphere Model: CAM3", *Journal of Climate* (*in press*)

- Crowley, T. J., 1984, "Atmospheric circulation patterns during glacial inception - a possible candidate", *Quaternary Research*, **21**, 105–110
- Crowley, Thomas J., North, Gerald R., 1990, *Paleoclimatology*, Oxford University Press, Inc., New York
- DeWeaver, E., Nigam, S., 2004, "On the forcing of ENSO teleconnections by anomalous heating and cooling", *Journal of Climate*, **17**, 3225–3235
- Dyke, A. S., Andrews, J. T., Clark, P. U., England, J. H., Miller, G. H., Shaw, J., Veillette, J. J., 2002, "The Laurentide and Innuitian ice sheets during the Last Glacial Maximum", *Quaternary Science Reviews*, **21**, 9–31
- Fanning, A. F., Weaver, A. J., 1996, "An atmospheric energy-moisture balance model: Climatology, interpentadal climate change, and coupling to an ocean general circulation model", *Journal of Geophysical Research*, **101**, 15 111–15 128
- Forsstrom, P. L., Sallasmaa, O., Greve, R., Zwinger, T., 2003, "Simulation of fast-flow features of the Fennoscandian ice sheet during the Last Glacial Maximum", *Annals of Glaciology*, **37**, 383–389
- Forsstrom, Pirjo-Leena, Greve, Ralf, 2004, "Simulation of the Eurasian ice sheet dynamics during the last glaciation", *Global and Planetary Change*, **42**, 59–81
- Glen, J. W., 1958, "The flow law of ice: a discussion of the assumptions made in glacier theory, their experimental foundations and consequences", *International Association of Hydrological Sciences*, **47**, 171–183
- Goosse, H., Renssen, H., 2004, "Exciting natural modes of variability by solar and volcanic forcing: idealized and realistic experiments", *Climate Dynamics*, **23**
- Gordon, C. T., Stern, W., 1982, "A description of the GFDL global spectral model", *Monthly Weather Review*, **110**, 625–644
- Greuell, W., Knap, W. H., 2000, "Remote sensing of the albedo and detection of the slush line on the Greenland ice sheet", *Journal of Geophysical Research - Atmospheres*, **105**, 15 567–15 576
- Hannachi, A., 2001, "Toward a nonlinear identification of the atmospheric response to ENSO", *Journal of Climate*, **14**, 2138–2149
- Huybrechts, P., 1990, "A 3-D model for the Antarctic ice sheet: a sensitivity study on the glacial-interglacial contrast", *Climate Dynamics*, **5**, 79–92
- Huybrechts, P., Janssens, I., Pocin, C., Fichfet, T., 2002, "The response of the Greenland ice sheet to climate changes in the 21st century by interactive coupling of an AOGCM with a thermomechanical ice-sheet model", *Annals of Glaciology*, **35**, 409–415
- Huybrechts, P., Gregory, J., Janssens, I., Wild, M., 2004, "Modelling Antarctic and Greenland volume changes during the 20th and 21st centuries forced by GCM time slice integrations", *Global and Planetary Change*, **42**, 83–105
- Jenssen, D., 1977, "A three-dimensional polar ice sheet model", *Journal of Glaciology*, **18**, 373–389

- Jóhannesson, T., Sigurdsson, O., Laumann, T., Kennett, M., 1995, "Degree-day glacier mass-balance modelling with application to glaciers in Iceland, Norway, and Greenland", *Journal of Glaciology*, **41**, 345–358
- Kim, S. J., 2004, "The effect of atmospheric CO<sub>2</sub> and ice sheet topography on LGM climate", *Climate Dynamics*, **22**, 639–651
- Knap, W. H., Oerlemans, J., 1996, "The surface albedo of the Greenland ice sheet: Satellite-derived and in situ measurements in the Sondre Stromfjord area during the 1991 melt season", *Journal of Glaciology*, **42**, 364–374
- Koutavas, A., Lynch-Stiaglitz, J., Marchitto, T. M., Sachs, J. P., 2002, "El Niño-like pattern in ice age tropical Pacific sea surface temperature", *Science*, **297**, 225–230
- Lunt, Daniel J., de Noblet-Ducoudr, Nathalie, Charbit, Sylvie, 2004, "Effects of a melted Greenland ice sheet on climate, vegetation, and the cryosphere", *Climate Dynamics*, **23**, 679–694
- Mahaffy, M. W., 1976, "A three-dimensional numerical model of ice sheets: tests on the Barnes Ice Cap, Northwest Territories.", *Journal of Geophysical Research*, **81**, 1059–1066
- Manabe, S., Broccoli, A. J., 1985, "The influence of continental ice sheets on the climate of an ice-age", *Journal of Geophysical Research - Atmospheres*, **90**, 2167–2190
- Marshall, S. J., Clark, P. U., 2002, "Basal temperature evolution of North American ice sheets and implications for the 100-kyr cycle", *Geophysical Research Letters*, **29**, Art. No. 2214
- Marshall, S. J., Tarasov, L., Clarke, G. K. C., Peltier, W. R., 2000, "Glaciological reconstruction of the Laurentide ice sheet: physical processes and modelling challenges", *Canadian Journal of Earth Sciences*, **37**, 769–793
- Marshall, Shawn J., Clarke, G. K. C., 1997, "A continuum mixture model of ice stream thermomechanics in the Laurentide Ice Sheet: (1) Theory", *Journal of Geophysical Research - Solid Earth*, **102**, 20 599–20 613
- Marshall, Shawn J., James, Thomas S., Clarke, Garry K. C., 2002, "North American Ice Sheet Reconstructions at the Last Glacial Maximum", *Quaternary Science Reviews*, **21**, 175–192
- Newman, M., Compo, G. P., Alexander, M. A., 2003, "ENSO-forced variability of the Pacific decadal oscillation", *Journal of Climate*, **16**, 3853–3857
- Otto-Bliesner, B. L., Marshall, S. J., Overpeck, J. T., Miller, G. H., Hu, A., 2006, "Simulating Arctic climate warmth and icefield retreat in the last interglaciation", *Science*, **311**, 1751–1753
- Pacanowski, R. C., Philander, S. G. H., 1981, "Parameterization of vertical mixing in numerical models of tropical oceans", *Journal of Physical Oceanography*, **11**, 1443–1451
- Pacanowski, R. C., Dixon, K., Rosati, A., 1991, "The GFDL Modular Ocean Model user guide", *Tech. rep.*, Princeton, N. J.
- Parizek, Byron R., Alley, Richard B., 2004, "Implications of increased Greenland surface melt under global-warming scenarios: ice-sheet simulations", *Quaternary Science Reviews*, **23**, 1013–1027

- Payne, A. J., 1998, "Dynamics of the Siple Coast ice streams, West Antarctica: results from a thermomechanical ice sheet model", *Geophysical Research Letters*, **25**, 3173–3176
- Peltier, W. R., 1985, "The LAGEOS constraint on deep mantle viscosity: results from a new normal mode method for the inversion of viscoelastic relaxation spectra", *Journal of Geophysical Research*, **90**, 9411–9421
- Petit, J. R., Jouzel, J., Raynaud, D., Barkov, N. I., Barnola, J. M., Basile, I., Bender, M., Chappellaz, J., Davis, J., Delaygue, G., Delmotte, M., Kotlyakov, V. M., Legrand, M., Lipenkov, V., Lorius, C., Pepin, L., Ritz, C., Saltzman, E., Stievenard, M., 1999, "Climate and atmospheric history of the past 420,000 years from the Vostok ice core, Antarctica", *Nature*, **399**, 429–436
- Philander, S. G., 1990, *El Niño, La Niña, and the Southern Oscillation*, Academic Press, San Diego
- Rasmusson, E. M., Carpenter, T. H., 1982, "Variations in tropical sea-surface temperature and surface wind fields associated with the Southern Oscillation El-Niño", *Monthly Weather Review*, **110**, 354–384
- Ridley, J. K., Huybrechts, P., Gregory, J. M., Lowe, J. A., 2005, "Elimination of the Greenland ice sheet in a high CO<sub>2</sub> climate", *Journal of Climate*, **18**, 3409–3427
- Roe, G. H., Lindzen, R. S., 2001, "The mutual interaction between continental-scale ice sheets and atmospheric stationary waves", *Journal of Climate*, **14**, 1450–1465
- Rosenthal, Y., Broccoli, A. J., 2004, "In Search of paleo-ENSO", *Science*, **304**, 219–221
- Sardeshmukh, P. D., Hoskins, B. J., 1988, "The Generation of Global Rotational Flow by Steady Idealized Tropical Divergence", *Journal of the Atmospheric Sciences*, **45**, 1228–1251
- Schneider, N., Comuelle, B. D., 2005, "The forcing of the Pacific decadal oscillation", *Journal of Climate*, **18**, 4355–4373
- Shinn, Richard A., Barron, Eric J., 1989, "Climate sensitivity to continental ice sheet size and configuration", *Journal of Climate*, **2**, 1517–1537
- Slonosky, V. C., Mysak, L. A., Derome, J., 1997, "Linking Arctic sea-ice and atmospheric circulation anomalies on interannual and decadal timescales", *Atmosphere-Ocean*, **35**, 333–366
- Stott, L., Poulsen, C., Lund, S., Thunell, R., 2002, "Super ENSO and global climate oscillations at millennial time scales", *Science*, **297**, 222–226
- Straus, D. M., Shukla, J., 2002, "Does ENSO force the PNA?", *Journal of Climate*, **15**, 2340–2358
- Trenberth, K. E., 1997, "The definition of El Niño", *Bulletin of the American Meteorological Society*, **78**, 2771–2777
- Trenberth, K. E., Caron, J. M., Stepaniak, D. P., Worley, S., 2002, "Evolution of El Niño-Southern Oscillation and global atmospheric surface temperatures", *Journal of Geophysical Research - Atmospheres*, **107**, Art. No. 4065

- Trombotto, D., Buk, E., Hernandez, J., 1997, "Monitoring of mountain permafrost in the Central Andes, Cordón del Plata, Mendoza, Argentina", *Permafrost and Periglacial Processes*, **8**, 123–129
- Tudhope, A. W., Chilcott, C. P., McCulloch, M. T., Cook, E. R., Chappell, J., Ellam, R. M., Lea, D. W., Lough, J. M., Shimmield, G. B., 2001, "Variability in the El Niño - Southern oscillation through a glacial-interglacial cycle", *Science*, **291**, 1511–1517
- van der Avoird, E., Dijkstra, H. A., Nauw, J. J., Schuurmans, C. J. E., 2002, "Nonlinearly induced low-frequency variability in a midlatitude coupled ocean-atmosphere model of intermediate complexity", *Climate Dynamics*, **19**, 303–320
- Wang, X., Auler, A. S., Edwards, R. L., Cheng, H., Cristaili, P. S., Smart, P. L., Richards, D. A., Shen, C.-C., 2004, "Wet periods in northeastern Brazil over the past 210 kyr linked to distant climate anomalies", *nature*, **432**, 740–743
- Wu, A., Hsieh, W. W., 2004, "The nonlinear patterns of North American winter temperature and precipitation associated with ENSO", *Journal of Climate*, **18**, 1736–1752
- Wu, P., Peltier, W. R., 1982, "Viscous gravitational relaxation", *Geophysical Journal of the Royal Astronomical Society*, **70**, 435–485
- Yin, J. H., Battisti, D. S., 2001, "The importance of tropical sea surface temperature patterns in simulations of last glacial maximum climate", *Journal of Climate*, **14**, 565–581